Manuscript Details

Manuscript number	EARTH_2018_356
Title	Sediment-Hosted Geothermal Systems: review and first global mapping
Article type	Review Article

Abstract

Sediment-Hosted Geothermal Systems (SHGSs) are hybrid geological systems, where geothermal and sedimentary domains interact, leading to mixtures of inorganic and organic gases. Typically characterized by geothermal (thermometamorphic or mantle-derived) CO2 and biotic (microbial or thermogenic) CH4, SHGSs occur in sedimentary basins crossed by magmatic intrusions or involved in volcanic plumbing systems. These systems can be of considerable interest for petroleum exploration and natural greenhouse-gas emission studies, but systematic studies for their characterization and worldwide distribution are missing. Here, we provide a review of SHGSs identified so far, and propose methodological criteria for their definition and identification, based on integrated geological and gas-geochemical parameters. We find that SHGSs are typically characterized by: (a) fluids dominated by mantle or decarbonation-methamorphic CO2 (>50 vol.%); (b) considerable amounts of CH4 and heavier hydrocarbons (at least 1.5 vol.%, generally up to 30-40 vol.%), produced by microbial or thermogenic degradation of organic matter hosted in sedimentary rocks; (c) tectonically active sedimentary basins (back-arc, rift zones and foredeep), generally hosting petroleum fields and within ~300 km from recent or ancient volcanic centers. This analysis resulted in a global map including a first set of 33 SHGSs located in North America, Central and Eastern Europe, Far East, Eastern Oceania and Northern New Zealand, and a second set of potential SHGS prone areas, occurring also in South America, North Africa, Middle East and Kamchatka. The present SHGS map can evolve on the basis of more detailed geological analysis and new gas-geochemical data.

Keywords	Sediment-Hosted Geothermal Systems; carbon dioxide; methane; sedimentary basins; volcanoes; geothermal systems; hydrocarbons; mapping

Corresponding Author	Monia Procesi
Corresponding Author's Institution	Istituto Nazionale di Geofisica e Vulcanologia
Order of Authors	Monia Procesi, Giancarlo Ciotoli, Adriano Mazzini, Giuseppe Etiope

Suggested reviewers	Yunyan Ni, Rick Allis, Henrik Svensen, Maciej Kotarba

Submission Files Included in this PDF

File Name [File Type]

Procesi Cover Letter_SHGS_ESR.doc [Cover Letter]

Abstract_Procesi_13072018.docx [Abstract]

Manuscript_Procesi_13072018.docx [Manuscript File]

Figure captions.docx [Figure]

Fig.1.tif [Figure]

Fig.2.tif [Figure]

Fig.3.tif [Figure]

Fig.4.tif [Figure]

Fig.5.tif [Figure]

Fig.6.tif [Figure]

Fig.7.tif [Figure]

Fig.8.tif [Figure]

Fig.9.tif [Figure]

TAB1_13072018.docx [Table]

TAB2_13072018.doc [Table]

TAB3_13072018.docx [Table]

TAB4_13072018.docx [Table]

Supplementary_Procesi_13072018.docx [Supporting File]

To view all the submission files, including those not included in the PDF, click on the manuscript title on your EVISE Homepage, then click 'Download zip file'.

July 13th, 2018

Dear Editor,

I am pleased to submit to *Earth Science Reviews* the manuscript entitled "**Sediment-Hosted Geothermal Systems: review and first global mapping"** by Procesi M., Ciotoli G., Mazzini A. & Etiope G.

The work reports a global review of the Sediment-Hosted Geothermal Systems (SHGS), namely, hybrid geological systems where geothermal and sedimentary domains interact, and proposes methodological criteria for their definition and identification, based on integrated geological and gas-geochemical parameters.
We tried to cover all the main aspects and uncertainties dealing with the problem of the hybrid systems, clarifying the terminology and proposing a methodological approach.
Specifically, we provide a review of previously identified SHGSs (Chapter 3) and propose geochemical and geological criteria for their identification and characterization (Chapter 4). We conclude outlining their specific environmental and energy resource implications (Chapter 5). Moreover, future directions for potential specific research are introduced - with clumped isotopes as a specific example.

We believe that our review is of interest for a wide scientific community including volcanologists, geochemists, petroleum geologists and sedimentologists.

Thanks for handling this manuscript.

On the behalf of all the Authors
Sincerely,

Monia Procesi

Istituto Nazionale di Geofisica e Vulcanologia
via Vigna Murata 605 00143 Roma
monia.procesi@ingv.it

Sediment-Hosted Geothermal Systems: review and first global mapping

Procesi M.[1], Ciotoli G. [2,1], Mazzini A.[3], Etiope G.[1,4]

[1] Istituto Nazionale di Geofisica e Vulcanologia, Via di Vigna Murata 605, 00143 Roma, Italy
[2] Istituto di Geologia Ambientale e Geoingegneria—CNR-IGAG, Roma, Italy Centre for Earth
[3] Centre for Earth Evolution and Dynamics (CEED), University of Oslo, Norway
[4] Faculty of Environm. Science and Engineering, Babes Bolyai University, Cluj-Napoca, Romania

Abstract

Sediment-Hosted Geothermal Systems (SHGSs) are hybrid geological systems, where geothermal and sedimentary domains interact, leading to mixtures of inorganic and organic gases. Typically characterized by geothermal (thermometamorphic or mantle-derived) CO_2 and biotic (microbial or thermogenic) CH_4, SHGSs occur in sedimentary basins crossed by magmatic intrusions or involved in volcanic plumbing systems. These systems can be of considerable interest for petroleum exploration and natural greenhouse-gas emission studies, but systematic studies for their characterization and worldwide distribution are missing.

Here, we provide a review of SHGSs identified so far, and propose methodological criteria for their definition and identification, based on integrated geological and gas-geochemical parameters. We find that SHGSs are typically characterized by: (a) fluids dominated by mantle or decarbonation-methamorphic CO_2 (>50 vol.%); (b) considerable amounts of CH_4 and heavier hydrocarbons (at least 1.5 vol.%, generally up to 30-40 vol.%), produced by microbial or thermogenic degradation of organic matter hosted in sedimentary rocks; (c) tectonically active sedimentary basins (back-arc, rift zones and foredeep), generally hosting petroleum fields and within ~300 km from recent or ancient volcanic centers. This analysis resulted in a global map including a first set of 33 SHGSs located in North America, Central and Eastern Europe, Far East, Eastern Oceania and Northern New Zealand, and a second set of potential SHGS prone areas, occurring also in South America, North Africa, Middle East and Kamchatka. The present SHGS map can evolve on the basis of more detailed geological analysis and new gas-geochemical data.

Sediment-Hosted Geothermal Systems: review and first global mapping

Procesi M.[1], Ciotoli G. [2,1], Mazzini A.[3], Etiope G.[1,4]

[1] Istituto Nazionale di Geofisica e Vulcanologia, Via di Vigna Murata 605, 00143 Roma, Italy
[2] Istituto di Geologia Ambientale e Geoingegneria—CNR-IGAG, Roma, Italy Centre for Earth
[3] Centre for Earth Evolution and Dynamics (CEED), University of Oslo, Norway
[4] Faculty of Environm. Science and Engineering, Babes Bolyai University, Cluj-Napoca, Romania

Abstract

Sediment-Hosted Geothermal Systems (SHGSs) are hybrid geological systems, where geothermal and sedimentary domains interact, leading to mixtures of inorganic and organic gases. Typically characterized by geothermal (thermometamorphic or mantle-derived) CO_2 and biotic (microbial or thermogenic) CH_4, SHGSs occur in sedimentary basins crossed by magmatic intrusions or involved in volcanic plumbing systems. These systems can be of considerable interest for petroleum exploration and natural greenhouse-gas emission studies, but systematic studies for their characterization and worldwide distribution are missing.

Here, we provide a review of SHGSs identified so far, and propose methodological criteria for their definition and identification, based on integrated geological and gas-geochemical parameters. We find that SHGSs are typically characterized by: (a) fluids dominated by mantle or decarbonation-methamorphic CO_2 (>50 vol.%); (b) considerable amounts of CH_4 and heavier hydrocarbons (at least 1.5 vol.%, generally up to 30-40 vol.%), produced by microbial or thermogenic degradation of organic matter hosted in sedimentary rocks; (c) tectonically active sedimentary basins (back-arc, rift zones and foredeep), generally hosting petroleum fields and within ~300 km from recent or ancient volcanic centers. This analysis resulted in a global map including a first set of 33 SHGSs located in North America, Central and Eastern Europe, Far East, Eastern Oceania and Northern New Zealand, and a second set of potential SHGS prone areas, occurring also in South America, North Africa, Middle East and Kamchatka. The present SHGS map can evolve on the basis of more detailed geological analysis and new gas-geochemical data.

Keywords: *Sediment-Hosted Geothermal Systems; carbon dioxide; methane; sedimentary basins; volcanoes; geothermal systems; hydrocarbons; mapping.*

Contents

1. Introduction

The release of carbon-bearing gases from the Earth is generally classified considering two distinct and broad geological domains: (a) the high temperature volcano-geothermal systems, releasing inorganic carbon dioxide (CO_2) rich gases, typically produced by thermometamorphism of limestones or magma-mantle degassing, and (b) the low temperature sedimentary basins, releasing mainly biotic methane (CH_4) and other hydrocarbons, produced by microbial or thermogenic degradation of organic matter or oil in sedimentary rocks. A wide body of literature exists about geochemistry and geology of such degassing processes, which have considerable implications for the environment, geo-hazards, global climate changes and energy resource exploration (e.g., relevant case-histories and reviews are reported by Klusman et al. 1998; Kerrick, 2001; Etiope and Klusman, 2002; Morner and Etiope, 2002; Chiodini et al. 2004; Burton et al. 2013; Etiope, 2015). In many cases, however, geothermal and sedimentary domains can partially overlap, leading to hybrid geological systems with mixtures of inorganic and biotic gases. These hybrid systems are known as *Sediment-Hosted Geothermal Systems* (SHGSs), or *Sediment-Hosted Hydrothermal Systems* (SHHS). We will use the first term, SHGS, discussing the reasons in Chapter 2. These systems refer to sedimentary basins perturbed by magmatic intrusions or involved in volcanic plumbing systems, and characterized by CO_2–rich geothermal fluids and biotic (microbial or thermogenic) CH_4, sourced from the organic-rich sediments. Inorganic CO_2 concentrations generally exceed 50 vol.%. CH_4 (and heavier alkanes, such as ethane and propane) concentrations are generally higher (roughly >1-2 vol.%) than those occurring in pure volcanic-geothermal fluids (typically in the order of ppbv or ppmv; Taran and Giggenbach, 2003; Capaccioni et al, 2004; Etiope et al, 2007; Fiebig et al, 2015). SHGSs are common, as palaeo-systems, in the large igneous provinces as those of South Africa, Australia, Siberia and the North Atlantic province (Jamtveit et al., 2004; Holford et al., 2013; Svensen et al., 2004; Svensen et al., 2007; Svensen et al., 2009; Jones et al., 2016; Reynolds et al., 2017). Active SHGSs are recognized in the Guaymas Basin Rift Zone-Gulf of California (Pacific Ocean; Welhan and Lupton, 1987; Berndt, C., et al., 2016), in the Salton Sea geothermal field in California (e.g., Helgeson, 1968; Mazzini et al., 2011), in Java, Indonesia (Lusi eruption; Mazzini et al 2012), within the Tiber Delta, at Fiumicino, in central Italy (Ciotoli et al. 2016) and in the Songliao Basin (Shuai et al., 2018). Their surface manifestations, like muddy craters or bubbling pools, may be similar to, and thus may be confused with, pure sedimentary gas manifestations (hydrocarbon seeps), such as mud volcanoes (Etiope, 2015; Mazzini and Etiope, 2017), or mere geothermal/volcanic manifestations (e.g., mofettes, bubbling pools, muddy geysers). The distinction between SHGSs, pure sedimentary systems and geothermal-volcanic complexes is not only a semantics problem. The attribution of SHGS implies, in fact, the

recognition of specific geological and geochemical processes that can have peculiar implications for petroleum exploration and global climate change studies. SHGSs, in fact, (1) may lead to production of hydrocarbons resulting from enhanced thermal maturity of sedimentary source rocks; (2) can be significant natural sources of greenhouse gas (CO_2 and CH_4) emissions to the atmosphere (Etiope, 2015), and (3) are potential driver of past climate changes (Svensen et al., 2004; Aarnes et al., 2010; Iyer et al., 2013; Polozov et al., 2016). Nevertheless, systematic studies for SHGS characterization and worldwide distribution are missing.

Here we provide a review of previously identified SHGSs (Chapter 3) and propose geochemical and geological criteria for their identification and characterization (Chapter 4). In particular gas genetic diagrams will show fundamental differences among classic CO_2-dominated (volcanic, hydrothermal) systems, CH_4-dominated (sedimentary) seepage systems, and SHGSs. These criteria are then used to identify and map other potential SHGSs on the globe (Chapter 4). We conclude outlining their specific environmental and energy resource implications (Chapter 5). The sequence of the logical flow chart of this approach is schematized in figure 1. It is important to highlight that most of the SHGSs identified so far (Guaymas Basin, Salton Sea, Lusi, Fiumicino Tiber-Delta) have been recognized based on the occurrence of surface gas manifestations. Nevertheless, the concept of SHGS is independent of surface gas discharges, which act only as "vehicle" of subsurface information. Obviously, deep-seated SHGSs may exist also without any surface expression, and they can be identified through deep boreholes, as in the case of the Songliao Basin. Accordingly, in this work, we have addressed the potential SHGSs revealed by both surface manifestations and borehole data.

*Proposed location for **Figure 1***

2. Definitions

The peculiarity of hybrid geological systems, with volcano-hydrothermal and sedimentary components, was recognized in early works in California, at the Salton Sea geothermal field (Helgeson, 1968), in the Gulf of California, at the Guaymas Basin (Von Damm et al., 1985; Welhan and Lupton, 1987) and, more recently, at Lusi in East Java (Mazzini et al., 2012), in central Italy within the Tiber Delta (Ciotoli et al., 2013; 2016) and in the Songliao petroliferous Basin in China (Shuai et al. 2018). These works noted that deep sedimentary basins crossed by magmatic fluids or igneous intrusions, may result in the migration of a combination of fluids, hot water and gases,

different from the one observed in classic volcanic-geothermal systems or classic sedimentary basins.

Several terms, such as sediment-hosted mineral deposits (Von Damm et al., 1985), sediment-dominated hydrothermal systems (Jamtveit et al., 2004), sediment-hosted low temperature systems (Nicholson, 1993), sediment-hosted hydrothermal systems (Mazzini et al., 2011) or sediment-hosted geothermal systems (Alt, 2009; Mazzini et al., 2011; Ciotoli et al., 2013; Di Pippo, 2016; Ciotoli et al., 2016; Mazzini and Etiope, 2017; Shuai et al., 2018) have been used to define this kind of geological setting; but a clear and univocal definition of these terms is still lacking.

The above Authors used the term *sediment,* referring to systems hosted in sedimentary rocks; whereas they often used "geothermal" or "hydrothermal" referring to emission of hot fluids. However, "geothermal" and "hydrothermal" have a different meaning as proposed by Jackson (1997). *Geothermal* refers to any system that transfers heat from within the Earth towards the surface, while *hydrothermal* is a subset of *geothermal*, implying that the heat transfer is manly operated by water (convection), in liquid or steam state. This is also defined as *Conventional Geothermal System (CGS)* to indicate a classic high heat flow hydrothermal system that typically includes the circulation of meteoric water that infiltrates and migrates to depths of several kilometers generating convective transport mechanisms (Heasler et al., 2009). Nevertheless, hydrothermal circulation is not always present in medium-high temperature (geothermal) areas and in sedimentary basins. For these reasons, we prefer to use the term "Sediment-Hosted *Geothermal* System*"* instead of "*Hydrothermal"*.

Some authors recently introduced the term "*Sedimentary Geothermal Resources*" referring to relatively "hot" sedimentary systems where geothermal energy can be exploited (for direct and/or indirect use; Jiachao, 2012; Porro et al., 2012; Anderson et al., 2013). In this framework, Rybach (1981) highlighted that the geothermal *resource* is formed by an economically sufficient amount of heat concentration at drillable depth of the Earth's crust, whereas the geothermal *system* is generally classified by its geological, hydrogeological and heat transfer characteristics. Therefore, the *Sedimentary Geothermal Resources* may lack the hybrid fluid features and, as a consequence, may exclude the SHGSs described in this review.

To better clarify the gas-geochemical and geological factors characterizing a SHGS, we briefly describe the active SHGSs identified so far (Guaymas Basin, Gulf of California; Salton Sea, California; Lusi, Indonesia; Tiber Delta – Fiumicino, Italy; Songliao Basin, China) (Fig. 2a-e), focusing on their strong analogies. These analogies will be used as reference for setting the geochemical-geological criteria for a general characterization and a first SHGS global screening (Chapter 4).

*Proposed approximate-location for **Figure 2***

(The Authors request full page image)

3. Previously identified SHGSs

3.1 Guaymas Basin (Gulf of California)

The Guaymas Basin is located in the central part of the Gulf of California (N27°03'; W111°07'). It is an actively spreading oceanic basin that is part of the system of spreading axes and transform faults extending from the East Pacific Rise to the San Andreas fault (Curray et al., 1982; Lonsdale and Becker, 1985) (Fig. 2a). The basin has a maximum depth of ~2000 m and consists of two NE oriented sub-basins that are 30 and 50 km long, respectively (Lonsdale and Becker, 1985). The lithology of the basin was assessed through a Deep Sea Drilling Project (Curray et al., 1982). Seismic studies indicate the presence of a magmatic chamber in the basin, below a sedimentary column, 700-1000 m thick (Curray et al., 1982), which rapidly covered the rift floor (sedimentation rate >2m/1000yr). The sequence includes basaltic sills in contact with diatomaceous, calcareous deposits rich in organic matter and detritic clay minerals (Von Damm et al., 1985 and references therein). The estimated geothermal reservoir temperature is 315°C (Von Damm et al., 1985) and the computed mean heat flow is 453 mW/m^2 (Curray et al., 1982). The chemical composition of the Guaymas fluids is typical of deep submarine "hot" vents, dominated by CO_2 (~90 vol.%) followed by CH_4 (~10 vol.%) (Simoneit and Galimov, 1984; Galvàn et al., 2015). In addition to the "magmatic" influence of the basaltic sills, the fluids also show effects of interaction with organic matter within the sediments (German and Von Damm, 2003; Berndt et al, 2016). Thermal stress caused rapid maturation of the organic matter with concomitant generation of oil and thermogenic hydrocarbon gas (Simoneit, 1988, Teske et al., 2016), as indicated by δ^{13}C-CH_4 data, ranging between -51 and -15‰ VPDB (Welhan and Lupton, 1987; Berndt et al, 2016). The fossil source of CH_4 is confirmed by radiocarbon measurements (^{14}C-CH_4) that show values of 0.2 ± 0.1 pMC (Kessler et al., 2008). The CO_2 carbon isotope data (ranging between -6 and +2.7‰ VPDB) suggest a source related to thermo-metamorphic reactions on carbonates and magma-mantle degassing (Welhan and Lupton, 1987).

3.2 Salton Sea (California)

The Salton Sea geothermal system is situated in the Salton Trough in southern California (N33°12'; W115°34'), an area with abundant surface hydrothermal manifestations (bubbling mud pools, gryphons and gas vents) (Svensen et al., 2007; Svensen et al., 2009; Mazzini et al., 2011). Salton Sea occurs in a pull-apart basin, filled by sedimentary rocks and intruded by quaternary basalt and rhyolite bodies, inducing high heat flow (up to 600 mW/m^2) (Svensen et al., 2007; Mazzini et al., 2011; Onderdonk et al., 2011) (Fig. 2b). The intrusions can cause a temperature increase exceeding 350°C at the depth of 1400m, diffuse CO_2 degassing and alteration of organic matter (Svensen et al., 2007). The chemical composition of gas discharged to the surface is dominated by CO_2 with concentrations up to 98 vol.%, followed by CH_4 (up to 1.9 vol.%) and heavier hydrocarbons (C_{2+}<0.5 vol.%). The $\delta^{13}C$-CO_2 (ranging from -5.4 to +0.4 ‰) is within the range of magmatic sources and thermal decarbonation reactions (Mazzini et al., 2011 and references therein), while $\delta^{13}C$-CH_4 (from -32 to -17.6 ‰) suggests a mixing of thermogenic and abiotic sources (Mazzini et al., 2011 and references therein).

3.3 Lusi (East Java)

The 29th of May 2006 boiling mud breccia, gas and water suddenly erupted in the Regency of Sidoarjo, along the Watukosek fault system in north east of Java, Indonesia (S7°44'; E112°34') (Mazzini et al., 2007). This eruption site was named Lusi, a contraction of Lumpur Sidoarjo wherein "Lumpur" is the Indonesian Bahasa word for mud. More than 12 years later, Lusi is still active erupting with a flow rate of ~80.000 m^3/day (early 2018; Miller and Mazzini, 2018). Lusi is located in a Tertiary-aged back-arc basin of NE Java (Kusumastuti et al., 2002), where the sedimentary sequences are characterized by high sedimentation rates of organic-rich deposits often capped by sealing units of tuffaceous or volcanoclastic sands. Mud volcanoes (= sedimentary volcanism) are widespread in this part of the island (Satiana 2008, Mazzini et al., 2009, Istadi et al., 2012) but Lusi has been recognized to have different characteristics from a mud volcano (Mazzini et al., 2012). Unlike the other classic mud volcanoes of Java, Lusi is situated in the proximity of the large Arjuno-Welirang volcanic complex. Here the geothermal gradient is relatively high (42°C/km) and the fluids erupted from the main crater are characterized by high concentrations of water vapour. Besides the water vapour, CO_2 is the main gas (>58 vol.% dry phase), and, with $\delta^{13}C$-CO_2 values between -2.2 and -12.8 ‰, is mostly associated to mantle-magma degassing and/or decarbonation processes, whereas methane, with concentration up to 40% (Mazzini et al., 2017) is related to thermogenic origin with $\delta^{13}C$-CH_4 from -31 to 51.8‰ (Mazzini et al., 2012; Mazzini et

al., 2017). Early isotopic data, collected soon after the eruption started, indicated the presence of an organic CO_2 component (Mazzini et al., 2012), interpreted as initial degassing contribution from the shallower sedimentary layers pierced by the active conduit. The thousands of satellite seeps scattered over kilometres around the crater (e.g. Sciarra et al., 2018) typically have higher CH_4 concentrations (up to 99 vol.%). Also in this case, methane has a biotic (thermogenic, mixed with microbial) origin ($\delta^{13}C$-CH_4 from -41 to 66 ‰) and CO_2 has inorganic origin (-8.2‰ $\leq\delta^{13}C$-$CO_2 \leq$ 4.12‰; Sciarra et al., 2018). Integrated geochemical geological and geophysical data are consistent with a SHGS scenario where deep seated (> 4000 m) magmatic intrusions and hydrothermal fluids migration are responsible for the enhanced heat that altered source rocks and/or gas reservoirs (Mazzini et al., 2012; Fallahi et al., 2017; Mazzini et al., 2018; Inguaggiato et al., 2018). (Fig. 2c).

3.4 Tiber Delta-Fiumicino (Italy)

The Tiber Delta, along the Tyrrhenian Sea margin in Central Italy (N12°26'; 41°76'), is located within the youngest back-arc basin of the Mediterranean region. It developed since the Miocene as a consequence of rifting and back arc extension associated with the west-dipping and "easterly" retreating Apennine subduction zone (Bigi et al., 2015 and references therein). Here the heat flow shows anomalous values, ranging from 100 to 200 mW/m^2 due to mantle uplift and/or crustal thinning (Scrocca et al., 2003). In 2013, a sudden eruption of CO_2-rich gas occurred in this area, near Fiumicino town and very close to the Rome's international airport (Ciotoli et al., 2013; Giordano et al., 2016). CO_2 vents and anomalous CO_2 and CH_4 concentrations in the soil have also been discovered at several sites within the delta (Ciotoli et al., 2016) (Fig. 2d). The gas is dominantly composed by inorganic/geothermal CO_2 (up to 98 vol.%; -2‰ $\leq \delta^{13}C$-$CO_2 \leq$ -0.7‰) and by minor amounts (up to 3.7 vol.%) of biotic (mainly thermogenic) CH_4 (-54‰ $\leq \delta^{13}C$-$CH_4 \leq$ -37‰). While CO_2 has the same origin of the geothermal gas of the adjacent Alban Hills volcano, CH_4 likely sourced from Meso-Cenozoic petroleum systems overlying deep magmatic fluids. Inorganic and biotic gases originated in different systems and depths, but follow the same migration pathways defined by active faults of a half-graben (Ciotoli et al., 2016).

3.5 Songliao Basin, Xujiaweizi Depression (China)

The Songliao Basin is a large intracontinental Mesozoic-Cenozoic sedimentary basin in northeastern China *(*N47°43'; E127°34'*)* (Fig. 2e). The evolution of the basin can be divided into four stages: mantle upwelling, rifting, post-rifting thermal subsidence and structural inversion. More

than 30 rift depressions, such as the Xujiaweizi depression, developed during the late Jurassic to early Cretaceous period (Feng, 2008). These isolated rift systems are characterized by volcanic and coal-bearing clastic rocks. The Xujiaweizi rift depression is located near the center of the Songliao Basin and is characterized by over mature hydrocarbon source rocks due to the high geothermal gradient of this rift system (37 to 46 °C/km, with a mean of 40°C/km; Liu et al., 2016). The abundant and mature source rocks, and the favorable structural conditions for the formation of reservoir and cap-rocks, lead to the formation of prolific petroleum systems with mixing between a CO_2-poor, relatively high maturity coal gas and a CO_2-dominated gas typical of geothermal systems (up to 91 vol.%; $\delta^{13}C$-CO_2 -4.4‰). Based mainly on ^{13}C-enrichments in alkanes (e.g. $\delta^{13}C$-CH_4 -26.9 ‰), several authors proposed that in the Xujiaweizi sub-basin, considerable amounts of hydrocarbons have an abiotic origin (Guo et al., 1997; Wang et al., 2009; Liu et al., 2016; Huang et al., 2004; Feng et al., 2008; Mi et al., 2010). More recent studies, based on CH_4 clumped-isotopes have suggested a methane formation temperature ($167^{\pm 18}$ °C to $213^{\pm 22}$ °C) that is much lower than that of magmatic gas generation processes, and therefore compatible with the high maturity of local source rocks (Shuai et al. 2018). The inorganic origin of CO_2 is confirmed, suggesting the existence of a migration pathway related to deep faults and fractures, which allows for the uprising of the magmatic-mantle fluids (CO_2 and He) towards hydrocarbon reservoirs. Accordingly, the deep formations of the Songliao Basin have been suggested to represent a typical case of SHGS (Shuai et al., 2018).

4. Preliminary criteria for SHGS identification and characterization

4.1 Constraints

The SHGSs previously described have important analogies and recurring features. All systems are in sedimentary basins characterized by the following factors:

(a) gas emissions to the surface, or gas reservoirs (as in the case of Songliao Basin) dominated by inorganic CO_2 associated with variable amounts of biotic CH_4, usually higher than 1.5 vol.%.

(b) basin located within a tectonically active region;

(c) anomalous heat flux (>50 mW/m^2);

(d) presence of sills and/or deep magma intrusions related to geothermal or volcanic systems;

(e) organic matter rich sediments with thickness exceeding 700 m;

These recurring features, which may represent the preliminary constraints to identify potential SHGSs, are discussed in more detail below.

4.1.1 Gas-geochemical constraints

The CO_2 carbon isotope signature, $\delta^{13}C\text{-}CO_2$, related to magma and mantle degassing, is generally between -8 ‰ and -4 ‰, and the one related to decarbonation reactions (thermomethamorphism) at high temperatures (> 250 °C) varies from -2 ‰ to +2 ‰ (e.g., Hoefs, 2015). The CO_2 produced by bacterial or thermal degradation of organic matter or hydrocarbon oxidation in sedimentary rocks has, instead, $\delta^{13}C\text{-}CO_2$ values typically ≤ -10 ‰ (e.g., Jenden et al., 1993; Hunt, 1996). Basically, a geothermal system is characterized by $\delta^{13}C\text{-}CO_2$ values ranging between -8 ‰ and +2 ‰. Sedimentary (petroleum-related) gas may also have CO_2 with positive $\delta^{13}C\text{-}CO_2$ values due to biodegradation of hydrocarbons and secondary methanogenesis (Pallasser, 2000), but their CO_2 concentration is relatively low (<20-30 vol.%; and obviously lower than CH_4 concentration). The SHGSs recognized so far have actually a CO_2 compatible with the inorganic origin (-8.9 ‰ ≤ $\delta^{13}C\text{-}CO_2$ ≤ +2.7 ‰). Accordingly, we will consider as a first constraint for SHGSs, a gas which is dominated by CO_2 (concentration above 50 vol.%) and $\delta^{13}C\text{-}CO_2$ between -8 and +2 ‰. We will consider also those sites where inorganic CO_2 is identified (and clearly discussed in the reference work) but mixed with a minor organic component, leading to slightly lower $\delta^{13}C\text{-}CO_2$ values.

Typically, volcanic sources, as well as the hydrothermal/geothermal systems (or conventional geothermal systems), discharge methane of dominant abiotic origin, generated by magmatic, post-magmatic high-temperature processes and Fischer-Tropsch Type (FTT) reactions (Fiebig et al 2007; Etiope and Sherwood Lollar, 2013). In particular, methane in pure and active magmatic, sediment-free systems, is characterized by isotopic signature ($\delta^{13}C\text{-}CH_4$) typically between -10 ‰ and -18 ‰ (e.g., Welhan, 1988; Botz et al. 2003) and a concentration generally ranging from 10^{-4} and 0.5 vol.%. Geothermal fluids from hydrothermal systems have methane concentrations between 0.01 and 1 vol.% and $\delta^{13}C\text{-}CH_4$ values between -17 ‰ and -29 ‰. Nevertheless, hydrothermal geothermal systems can also release variable amounts of biotic methane, generally thermogenic, leading the total CH_4 concentration to exceed 1 vol.%. Thermogenic methane has $\delta^{13}C\text{-}CH_4$ values typically ranging from −55 to −30 ‰, even though highly mature gas may reach values of −20 ‰ (Schoell, 1988; Shuai et al., 2018) and low maturity gas can have $\delta^{13}C\text{-}CH_4$ values down to -75 ‰ (Milkov and Etiope, 2018). Microbial methane is normally characterized by $\delta^{13}C$ values lower than −55 ‰ (Whiticar, 1999). Thermogenic methane is also associated with higher gaseous hydrocarbons (ethane to butane) and oil, whose concentrations are variable according to the maturity of the source rock.

The SHGSs recognized so far have actually CH_4 concentrations exceeding 1 vol.% with isotopic composition compatible with a biotic (thermogenic) origin (-54 ‰ ≤ $\delta^{13}C$-CH_4 ≤ -24 ‰), produced by thermal maturation of organic matter or oil cracking in the sediments.

Combining in Normal Probability Plots (NPP) CH_4 concentration and $\delta^{13}C$-CH_4 data of known SHGSs and those of geothermal-volcanic sites (Supplementary Material) (Fig. 3a-b), we verified the presence of two populations divided by threshold values of 1.5 vol.% and approximately -30 ‰, respectively. These thresholds can be considered as statistical constraints of hypothetical SHGS population and will be taken into account for further identification of SHGSs, although in particular cases, as discussed above, $\delta^{13}C$-CH_4 of SHGSs can be higher than -30 ‰. For these systems, detailed geochemical studies are necessary to investigate the source of methane and the generation mechanisms, as done for the case of the Songliao Basin, whose thermogenic gas identification was possible thanks to clumped-isotope analyses (Shuai et al. 2018).

Proposed location for ***Figure 3a-3b***

4.1.2 Geological constraints

SHGSs have a hybrid geological and geochemical configuration, and are therefore half-way between a hydrothermal (conventional) geothermal system *sensu strictu* and a hydrocarbon-bearing sedimentary system. Such a configuration can occur within sedimentary basins in geodinamically active regions, especially those related to extensional domains as rift, back-arc and forearc basins, both onshore and offshore. SHGSs may be characterized by the presence of magma chambers or igneous intrusions (sills and/or dikes), in proximity of active volcanoes or close to hydrothermal areas characterized by medium-high temperatures and anomalous heat flux. The sedimentary domain, hosting the "geothermal" system, can be characterized by rocks rich in organic matter, more or less evolved into mature source rocks, or by complete petroleum systems, including source, reservoir and cap-rocks. The simultaneous occurrence of such "geothermal" and "sedimentary" features, in variable combinations, is a requisite for the identification of a SHGS (Fig. 4).
Accordingly, it is expected that those gas-geochemical features defined in Section 4.1.1 actually occur in the above described geological settings.

Proposed location for ***Figure 4***

4.2 Identification of new SHGSs

4.2.1 A new list of potential SHGSs

According to what has been discussed above, the identification of potential SHGSs has been carried out starting from a global selection of the CO_2 dominant gas discharges, in surface manifestations and boreholes, with ^{13}C-depleted CH_4 ($\delta^{13}C \leq$ -30 ‰) exceeding 1.5 vol.%. More than 200 published works have been examined. The works that report complete CO_2 and CH_4 composition and isotopic data, fulfilling the constraints established above, are listed in Table 2. For the sites that had more than one data set acquired in different times, the mean values have been considered.

In addition to the previously described SHGSs (Guaymas Basin, Salton Sea, Lusi, Tiber Delta-Fiumicino and Songliao Basin), 33 new sites have been identified (Tab.2; Fig. 5).

The newly identified SHGSs are located in the USA (California, Wyoming, Colorado, West Virginia; n. 2, 3, 13, 14, 15, 16, 24, 25, 36, 37, 38), Italy (7, 8), Hungary (26, 27), Slovenia (28), Poland (33), Taiwan (6, 34), Thailand (17, 18, 19, 35), China (21, 22, 23), Australia (29, 30, 31) and New Zealand (11, 12, 32) (Fig. 5).

Proposed location for ***Figure 5***

The gas-geochemistry features of the 38 selected SHGSs (newly and previously identified) are shown in the molecular and isotopic composition diagrams of Fig.6 a-d, where they are compared with volcanoes, conventional geothermal systems (CGS) and hydrocarbon systems. Volcanic-geothermal gas data are reported in *Supplementary Material*.

Figures 6a and 6b clearly highlight the hybrid geochemical characteristics of the SHGSs compared to volcanoes, CGS and hydrocarbon systems. It is worth noting that about 15 volcanic-geothermal sites have high CH_4 concentrations, exceeding 1.5 vol% (Fig. 6a). Isotopic data from these sites, however, are not available and we could not label them as SHGSs. Therefore, these sites would deserve further investigations. The inorganic origin of CO_2 (with possible minor organic component in some cases) is mainly related to magma degassing (Fig. 6c). The biotic origin of CH_4 is mainly related to high-maturity source rocks (Fig. 6d), as expected because of the influence of the relatively high temperatures. Salton Sea and Songliao Basin (n. 4, 20) gases are the systems with more ^{13}C-enriched thermogenic CH_4, corresponding to high maturity source rocks. In Songliao the hydrocarbon generation temperatures reached 230 °C (Shuai et al., 2018). A few low maturity (T_{LM}) gases, related to the first stages of catagenesis and to mixing of thermogenic and microbial gas, occur (e.g., Laghi del Vescovo, n. 10). Three SHGSs seem to involve methane of dominant

microbial origin (Australian sites n. 29-30-31, Colliery, Darkes Forest and Collinsville, respectively).

Proposed location for ***Figure 6a-6d***

4.2.2 Spatial analysis and mapping of SHGS prone areas

To identify additional potential SHGS prone areas, we spatially and statistically analysed the peculiar geological features characterizing the identified SHGSs described above, i.e. (a) heat flow, (b) sediment thickness of the basins, (c) distance from volcanic systems and (d) distance from hydrocarbon fields.

Spatial analysis of all collected data were conducted in GIS environment by using ArcGIS-10.5 version (copyright © 1999-2016 ESRI Inc.). The point layer relative to the identified SHGSs was overlaid on the geological features listed above and pointed out with the letters (a), (b), (c) and (d). The sources of these geological layers, in raster and vector format, are:

a) Heat flux map (1°x 1° grid resolution), obtained from the Global Heat Flow Database of the International Heat Flow Commission (Global Heat Flow Database);

b) Sediment thickness, derived from the Global Sediment Map (1°x 1° grid resolution) by Laske and Masters (1997);

c) Volcanoes of the World Geodatabase (Global Volcanism Program, 2013);

d) Hydrocarbon fields, from PETRODATA Dataset (Päivi et al., 2007).

The *extract multivalues to points* tool in ArcGIS was used to assign the values of the grid layers (a) and (b), to the SHGS point layer. Whereas, the *near distance* tool was used to calculate the distance of each SHGS from the nearest volcano and from the boundary of the nearest hydrocarbon field. Obtained data are presented in Table 3.

In order to define the range of population variability of each parameter (a), (b), (c) and (d), the 95% confidence limits for the mean were calculated (Table 4). These limits were used to categorize the variables (a), (b), (c) and (d) adopting a binary code “0” and “1”, outside and within the 95% confidence limit, respectively. The categorization was necessary to apply a multiple correspondence analysis (MCA) to define the association among the variable categories and to recognize those with similar profile. In particular, MCA highlights that (a), (c) and (d) with code “1” are correlated, while (b) is an independent variable (Fig. 7). Therefore, the co-existence of the three factors (a), (c) and (d) within the 95% confidence interval represents a first important diagnostic constraint for the occurrence of SHGS prone areas. In these areas, the existence of fluids, in seeps or reservoirs, with the geochemical characteristics discussed above, is probable but shall be investigated successively.

In order to map prone SHGS areas, the geological layers (a), (c) and (d) were classified, by Raster Calculator tool in ArcGIS, into binary grids using "0" and "1" codes, outside and within the 95% confidence limit, respectively. The binary grids were then summed to obtain a map of potential SHGS areas (Fig. 8). Since the SGHS are by definition within in a sedimentary basin, the obtained output raster was back-transformed in a vector polygon layer and intersected with Sedimentary Basins of the World Map (Robertson Basins and Plays - Tellus TM).

The resulting intersection map represents the global distribution of the SHGS prone areas. These areas are located in:

- western regions of North America, especially in the Great Plain Basin, and in the fore-arc and back-arc basins of the western part of South America, (i.e. Arauco Lebu, Linares Temuco, san Jorge, Magallanes and Ucayali);
- Europe, in the Italian neogenic basins (i.e. southern Po Plain, Ripi, Gela and Hyblean foreland), in the divergent basins around the Massif Central (i.e. basin of Paris, Rhine, Aquitaine and Bresse), in the Pannonian Basin, in part of the Southern and Northern Aegean Basin and in Central Turkey (Adana basin);
- Northern Africa and in particular in the intracratonic basins of Illizi Ghadames, Douela, Rio, central Atlas and western Sahara;
- Middle East, in the divergent basins of Sana, Tabuk and central Iran;
- part of the Far East, in particular in the divergent chinese basin of Shauxi and Subei, in the malaysian retro-arc basins of Greater Sorawak and Pamusian Tarakan, in the fore-arc Visayan Basin (Philippines), in the back and fore-arc basins of northern Japan (Niigata-Akita basins);
- back-arc basin of Western Kamchatka;
- Eastern Oceania and Northern New Zealand, in particular in the Otway and Taranaki basin.

The occurrence in these areas of fluids with SHGS characteristics (defined in section 4.1.1) shall be investigated in future detailed research.

*Proposed location for **Figure 7***

*Proposed location for **Figure 8** (The Authors request full page image)*

5. Environmental and energy resource implications of SHGSs

As anticipated in Introduction (chapter 1), SHGSs may have implications for energy resource exploration, and global climate change studies. SHGSs can in fact host source rocks with enhanced thermal maturity. In certain cases, it is possible that the development of hydrocarbons in the sedimentary rocks is facilitated by anomalous thermal regimes. These hydrocarbon systems may not occur in conventional petroleum system settings, and as such they may not be considered within the standard target areas of petroleum exploration. Therefore, SHGSs can represent frontier resources for natural gas exploration. The over-mature source rocks, induced by anomalous thermal status, typically release dry gas, characterized by high methane/ethane+propane ratios. Such high ratios could be misinterpreted as due to microbial origin but isotopic analyses shall be always performed to determine the gas origin. In addition, the exploitation of the SHGSs could open new energy scenarios such as the development of the co-produced system that use water-waste from oil gas fields for indirect and direct geothermal application. The co-produced systems for direct geothermal uses (i.e. district heating) have been successfully employed in some basins as the Pannonian (Hungary) and Paris Basin (France), which actually have been identified as potential SHGS areas in our analysis (see Fig.8), whereas for the indirect applications (power production) this technology is yet scarcely developed.

Moreover, SHGSs can be a significant natural source of greenhouse gas (CO_2 and CH_4) for the atmosphere. The importance and meaning of these gases, and their natural sources, in climate studies are discussed in a wide body of literature (e.g., Ciais et al., 2013). Surface manifestations of hydrocarbons (seepage) are today recognized as a major natural source of atmospheric methane (e.g., Ciais et al., 2013; Etiope, 2012; Schwietzke et al. 2016). These sources, however, included only mere sedimentary (gas-oil seeps, mud volcanoes) and geothermal-volcanic manifestations (mofettes, fumaroles, volcano-crater degassing), and SHGSs have not been specifically considered.

SHGS degassing dynamics may have a peculiar role in this respect. CH_4 occurring within the sedimentary sequences may not have sufficient pressure to migrate autonomously but it can reach the surface thanks to the occurrence of CO_2 flows, which is typical of SHGSs. Therefore, the CH_4 "stripping" process operated by CO_2 is a peculiar feature of SHGSs. Gas flux surveys in SHGSs worldwide may contribute to better estimate the global geological CH_4-CO_2 emissions to the atmosphere.

We note, then, that SHGSs can represent specific hazardous sites due to the explosive properties of methane. Methane can lead to explosions when its concentration is in a range of approximately 5–10 vol.% in the presence of oxygen. A level of 5 vol.% is referred to as the Lower Explosive Limit (LEL). A concentration of 0.5 vol.% CH_4, (i.e., 10% of the LEL), should be considered the limit

above which mitigation measures must be taken (Etiope, 2015). In many instances (see Table 2, Fig. 6a-6b), the concentrations of CH_4 in SHGSs may approach the explosive range, whereas CH_4 concentration in pure geothermal and petroliferous (oil or gas) seeps is generally outside this range.

6. Conclusions

This work provides a review of Sediment-Hosted Geothermal Systems (SHGSs), and proposes methodological criteria for their definition and identification, based on integrated geological and geochemical factors. SHGSs are hybrid systems where geothermal and sedimentary domains interact, leading to mixtures of inorganic and biotic gases, with relevant environmental and energy resource implications (Fig. 9). A few SHGSs recognized in previous works resulted to have important analogies and recurring features, which have been used as preliminary constraints to identify new potential SHGSs. The analogies include the existence of gas flows dominated by inorganic CO_2 associated with variable amounts of biotic (microbial or thermogenic) CH_4, usually > 1.5 vol.%, occurring within sedimentary basins in tectonically active regions, with anomalous heat flow (mainly between 80 and 160 mW/m^2) due to the presence of geothermal or volcanic systems, sills and/or deep magma intrusions. Examining CO_2-rich systems known in the literature, the peculiar gas-geochemical features (isotopic and molecular) of SHGSs previously recognized have been used as first diagnostic tool to identify 33 new SHGSs in Northern America, Europe, Asia and Oceania. Statistical and spatial analysis of geological data related to the 33 SHGSs, including heat-flow, sediment thickness and geographic distances from volcanic centers and petroleum fields, allowed to map additional, potential SHGS areas in all continents.

The potential SHGS areas mapped in this work can represent zones of significant emission of methane to the atmosphere, potential sites with gas-hazard, and new targets for petroleum and geothermal exploration. This SHGS map can be refined on the basis of more detailed geological analysis and new gas-geochemical data. CH_4 clumped-isotopes, in particular, can be beneficial in the assessment of methane origin, which is still ambiguous in several cases, distinguishing between thermogenic gas (produced up to 250°C) and magmatic or post-magmatic gas (produced at T>300-400°).

*Proposed location for **Figure 9***

Acknowledgements

This work is a contribution to the Deep Energy Community of the Deep Carbon Observatory.

References

Aarnes, I., Svensen H., Connolly J. A. D., and Podladchikov Y.Y. (2010) - How contact metamorphism can trigger global climate changes: Modeling gas generation around igneous sills in sedimentary basins, Geochim. Cosmochim. Acta, 74, 7179–7195.

Alt J.C. (2009) – Very low-grade hydrothermal metamorphism of basic igneous rocks. Editors: Frey M., Robinson D. In: Low-Grade Metamorphism. Ed. Wiley. Ch 6.

Anderson T.C. (2013) - Geothermal Potential of Deep Sedimentary Basins in the United States. GRC Transactions, Vol. 37.

Bennet S. (2011) - Geothermal Potential of Transtensional Plate Boundaries. GRC Transactions, Vol. 35, 2011

Bergfeld D., Goff F., Janik C. (2001) – Carbon isotope systematics and CO_2 sources in The Geysers-Clear Lake region, northern California, USA. Geothermics 30, 303-331.

Berndt, C., C. Hensen, C. Mortera-Gutierrez, S. Sarkar, S. Geilert, M. Schmidt, V. Liebetrau, R. Kipfer, F. Scholz, M. Doll, S. Muff, J. Karstens, S. Planke, S. Petersen, C. Böttner, W.-C. Chi, M. Moser, R. Behrendt, A. Fiskal, M.A. Lever, C.-C. Su, L. Deng, M.S. Brennwald, D. Lizarralde (2016) - Rifting under steam—How rift magmatism triggers methane venting from sedimentary basins: Geology, v. 44, p. 767-770

Bigi, S., Beaubien, G., Ciotoli, S., D'Ambrogi, C., Doglioni, C., Ferrante, V., Lombardi, S., Milli, S., Orlando, L., Ruggiero, L., Tartarello, M.C., Sacco P., (2015) - Mantle-derived CO2 migration along active faults within an extensional basin margin (Fiumicino, Rome, Italy). Tectonophysics 637, 137-149.

Bonini M., Sani F., Stucchi E.M., Moratti G. , Benvenuti M., Menanno G., Tanini C. (2014) - Late Miocene shortening of the Northern Apennines back-arc. Journal of Geodynamics 74, 1– 31.

Botz R., Wehner H., Schmitt M., Worthington T.J., Schmidt M., Stoffers P. (2002) - Thermogenic hydrocarbons from the offshore Calypso hydrothermal field, Bay of Plenty, New Zealand. Chemical Geology 186, 235– 248

Burton, M. R., G. M. Sawyer, and D. Granieri (2013) - Deep carbon emissions from volcanoes, Rev. Mineral. Geochem., 75, 323–354.

Capaccioni B., Y. Taran, F. Tassi, O. Vaselli, G. Mangani, and J. L. Macias (2004) - Source conditions and degradation processes of light hydrocarbons in volcanic gases: an example from El Chichon volcano (Chiapas State, Mexico). Chem. Geol., 206, 81–96.

Caracausi A., Italiano F., Nuccio P. M., Paonita A., Rizzo A., (2003) - Evidence of deep magma degassing and ascent by geochemistry of peripheral gas emissions at Mount Etna (Italy): Assessment of the magmatic reservoir pressure. J. Geophys. Res., 108, B10, 2463, doi: 10.1029/2002JB002095.

Carapezza M. L., TArchini L., Granieri D., Martelli M., Gattuso a., Pagliuca N., Ranaldi M., Ricci T., Grassa F., Rizzo A., (2015) - Gas blowout from shallow boreholes near Fiumicino International Airport (Rome): Gas origin and hazard assessment, Chem. Geol., 407–408, 54–65.

Carminati E. & Doglioni C. (2012) - Alps vs. Apennines: The paradigm of a tectonically asymmetric Earth. Earth Science Reviews 112, 67–96.

Ciais, P., et al. (2013), Carbon and other biogeochemical cycles, in Climate Change 2013: The Physical Science Basis. Contribution of Working Group I to the Fifth Assessment Report of the Intergovernmental Panel on Climate Change, edited by T. F. Stocker et al., Cambridge Univ. Press, Cambridge, U. K., and New York.

Chiodini, G., C. Cardellini, A. Amato, E. Boschi, S. Caliro, F. Frondini, and G. Ventura (2004) - Carbon dioxide Earth degassing and seismogenesis in central and southern Italy, Geophys. Res. Lett., 31, L07615, doi:10.1029/2004GL019480.

Ciotoli, G., G. Etiope, F. Florindo, F. Marra, L. Ruggiero, and P. E. Sauer (2013), Sudden deep gas eruption nearby Rome's airport of Fiumicino, Geophys. Res. Lett., 40, 5632–5636, doi:10.1002/2013GL058132.

Ciotoli, G., G. Etiope, F. Marra, F. Florindo, C. Giraudi, and L. Ruggiero (2016), Tiber delta CO_2-CH4 degassing: A possible hybrid, tectonically active Sediment-Hosted Geothermal System near Rome, J. Geophys. Res. Solid Earth, 121, doi:10.1002/2015JB012557

CGG, 2015 - Organic Geochemistry Data From FRogi and the Fluid Features Database.

Curray J.R., Moore D.G., Kelts D., Einsele G. (1982) - Tectonics and geological history of the passive continental margin at the tip of Baja California. In: Moore, et al. (Eds.), Initial Reports of the Deep Sea Drilling Project, Vol. 64, 1089-1116.

Dai J., Hu G., Ni Y., Li J., Luo X., Yang C., Hu A., Zhou Q. (2009) Distribution Characteristics of Natural Gas in Eastern China. Natural Gas Geoscience, 20, 4. (in Chinese language)

Della Vedova B., Bellani S., Pellis G. and Squarci P. (2001) – Deep temperatures and surface heat flow distribution. In: Anatomu of an Orogen: The Apennines and Adjacent Mediterranean Basins, 65-76. Vai and Martini (eds.). Ed. Kluwer.

Di Pippo R. (2016) - Geothermal Power Generation. Developments and Innovation. Ed. Woodhead Publishin, pp. 854, ISBN: 9780081003374

Etiope G. & Klusman R. (2002) - Geologic emissions of methane to the atmosphere. Chemosphere 49, 777–789.

Etiope G., Fridriksson T., Italiano F., Winiwarter W., Theloke J. (2007) - Natural emissions of methane from geothermal and volcanic sources in Europe. Journal of Volcanology and Geothermal Research 165, 76–86.

Etiope G., Feyzullayev A., Baciu C.L. (2009) - Terrestrial methane seeps and mud volcanoes: A global perspective of gas origin. Marine and Petroleum Geology 26, 333– 344.

Etiope G., Drobniak A., Schimmelmann A. (2012) - Natural seepage of shale gas and the origin of "eternal flames" in the Northern Appalachian Basin, USA. Marine and Petroleum Geology 43, 178-186.

Etiope, G., and Sherwood Lollar B., (2013) - Abiotic methane on Earth, Rev. Geophys., 51, 276–299, doi:10.1002/rog.20011.

Etiope (2015) - In: Natural Gas seepage. Edited by Springer ISBN 978-3-319-14601-0 (eBook) DOI 10.1007/978-3-319-14601-0 pag.1-199

Etiope G. (2017) – Natural Gas. In: Encyclopedia of Geochemistry. Ed.: W.M. White, Springe, DOI 10.1007/978-3-319-39193-9_152-1

Kessler J. D., Reeburgh W. S., Valentine D. L., Kinnaman F. S., Peltzer E. T., Brewer P. G., Southon J., and Tyler S. C. (2008) A survey of methane isotope abundance (14C, 13C, 2H) from five nearshore marine basins that reveals unusual radiocarbon levels in subsurface waters. Journal of Geophysical Research, Vol. 113, doi:10.1029/2008JC004822.

Fallahi, M. J., Obermann, A., Lupi, M., Karyono, K., and Mazzini, A., 2017, The Plumbing System Feeding the Lusi Eruption Revealed by Ambient Noise Tomography: Journal of Geophysical Research: Solid Earth, v. 122, p. 8200-8213.

Feng, Z.Q., 2008. Volcanic rocks as prolific gas reservoir: a case study from the Qing-shen gas field in the Songliao Basin, NE China. Mar. Pet. Geol.25, 416–432.

Fiebig, J., Woodland, A.B., Spangenberg, J., Oschmann, W., (2007) - Natural evidence for rapid abiogenic hydrothermal generation of CH_4. Geochimica et Cosmochimica Acta 71, 3028–3039.

Fiebig, J., Hofmann, S., Tassi, F., D'Alessandro, W., Vaselli, O., and Woodland, A.B. (2015) Isotopic patterns of hydrothermal hydrocarbons emitted from Mediterranean volcanoes. Chemical Geology 396, 152-163.

Galván C. A., Prol-Ledesma R. M., Torres-Vera M. A. (2015) - Geothermal prospects in the Baja California Peninsula. Geothermics, 39-57 http://dx.doi.org/10.1016/j.geothermics.2015.01.005

German C. R. & Von Damm K. L. (2003) - Hydrothermal Processes. In: Treatise on Geochemistry ISBN: 0-08-043751-6, Volume 6; (ISBN: 0-08-044341-9); pp. 181–222.

Giggenbach W.F. (1997) - Relative importance of thermodynamic and kinetic processes in governing the chemical and isotopic composition of carbon gases in high-heatflow sedimentary basins. Geochimica et Cosmochimica Acta, Vol. 61, No. 17, pp. 3763-3785,

Giordano, G., Carapezza, M.L., Monica, G. Della, Todesco, M., Tuccimei, P., Carlucci, G., De Benedetti, A.A., Gattuso, A., Lucchetti, C., Piersanti, M., Ranaldi, M., Tarchini, L., Pagliuca, N.M., Ricci, T., Facchini, S., D'Ambrosio, F., Misuraca, M., Bonamico, A., Geshi, N., 2016 Conditions for long-lasting gas eruptions: The 2013 event at Fiumicino International Airport (Rome, Italy), Journal of Volcanology and Geothermal Research, doi: 10.1016/j.jvolgeores.2016.06.020.

Global Heat Flow Database - http://www.datapages.com/gis-map-publishing-program/gis-open-files/global-framework/global-heat-flow-database/global-heat-flow-database) last download January 2018.

Global Volcanism Program, 2013. Volcanoes of the World, v. 4.6.6. Venzke, E (ed.). Smithsonian Institution. Downloaded 16 Mar 2018

Grassa F., Capasso g., Favara R., Inguaggiato S., Faber S., Valenza M. (2004) - Molecular and isotopic composition of free hydrocarbon gases from Sicily, Italy. Geophysical Research Letters, 31, L06607, doi:10.1029/2003GL019362.

Guo, Z., Wang, X., Liu, W., 1997. Reservoir-forming features of abiotic origin gas in Songliao Basin. Sci. China, Ser. D40, 621–626.

Heasler H., Jaworowski C., Foley D., (2009) - Geothermal systems and monitoring hydrothermal festures. in Young, R., and Norby, L., eds., Geological Monitoring: Boulder, Colorado, Geological Society of America, p. 105–140, doi: 10.1130/2009.monitoring.

Helgeson, H. C. (1968), Geologic and thermodynamic characteristics of Salton Sea geothermal system, Am. J. Sci., 266, 129–166.

Hoefs J. (2015) - Stable isotope geochemistry. Ed. Springer. ISBN: 978-3-319-19715-9, doi 10.1007/978-3-319-19716-6

Holford, S. P., Schofield N., Jackson C. A.-L., Magee C., Green P. F., and Duddy I. R., (2013) - Impacts of igneous intrusions on source and reservoir potential in prospective sedimentary basins along the Western Australian Continental Margin, in The Sedimentary Basins of Western Australia IV. Proceedings of the Petroleum Exploration Society of Australia Symposium, edited by M. Keep and S. J. Moss, Perth, Wash.

Huang, H., Yang, J., Yang, Y., Du, X., 2004. Geochemistry of natural gases in deep strata of the Songliao Basin, NE China. Int. J. Coal Geol.58, 231–244.

Hulston J.R., Hilton D.R., Kaplan I.R. (2001) - Helium and carbon isotope systematics of natural gases from Taranaki Basin, New Zealand. Applied Geochemistry 16, 419-436.

Hunt J.M. (1996) - Petroleum Geochemistry and Geology. (2nd ed.) W.H. Freeman Co., New York, 743 pp.

Iyer, K., Rupke L., and Galerne C. Y. (2013), Modeling fluid flow in sedimentary basins with sill intrusions: Implications for hydrothermal venting and climate change, Geochem. Geophys. Geosyst., 14, 5244–5262, doi:10.1002/2013GC005012.

Inguaggiato, S., Mazzini, A., Vita, F., and Sciarra, A., 2018, The Arjuno-Welirang volcanic complex and the connected Lusi system: Geochemical evidences: Marine and Petroleum Geology, v. 90, p. 67-76.

Jackson JA, Bates RL - 1997 - Glossary of Geology. American Geological Institute

Jamtveit B., Svensen H., Podladchikov Y.Y. & Planke S. (2004) - Hydrothermal vent complexes associated with sill intrusions in sedimentary basins. In: Breitkreuz. C. & Petford, N. (eds) 2004. Physical Geology of High-Level Magmatic Systems. Geological Society, London, Special Publications, 234, 233-241.

Jenden P.D, Newell K.D., Kaplan I.R., Watney W.L. (1988) Composition and stable isotope geochemistry of natural gases from midcontinent, U.S.A. Chem. Geol. 71, 117-147, doi:10.1016/0009-2541(88)90110-6.

Jenden P.D., Hilton D.R., Kaplan I.R. & Craig H., (1993) - Abiogenic hydrocarbons and mantle helium in oil and gas fields. The future of energy gases. U.S. Geological Survey Professional paper 1570.

Jiachao H. (2012) - Assessment and management of sedimentary geothermal resources. Master Thesis, Faculty of Earth Sciences University of Iceland

Jones, M.T., Jerram, D.A., Svensen, H.H., Grove, C., 2016. The effects of large igneous provinces on the global carbon and sulphur cycles. Palaeogeogr. Palaeoclimatol. Palaeoecol. 441, 4–21.

Kerrick D.M. (2001) - Present and past non-anthropogenic CO_2 degassing from the solid earth. Rev Geophys 39(4), 565-585

Kessler J. D., Reeburgh W. S., Valentine D. L., Kinnaman F. S., Peltzer E. T., Brewer P. G., Southon J. and Tyler S. C., (2008) - A survey of methane isotope abundance (^{14}C, ^{13}C, ^{2}H) from five nearshore marine basins that reveals unusual radiocarbon levels in subsurface waters. Journal of Geophysical Research, 113, doi:10.1029/2008JC004822.

Kotarba M.J., Rice D.D. (2001) – Composition and origin of coalbed gases in the Lower Silesian basin, southwest Poland. Applied Geochemistry, 16, 895-910.

Klusman, R.W., Jakel, M.E., LeRoy, M.P., (1998) - Does microseepage of methane and light hydrocarbons contribute to the atmospheric budget of methane and to global climate change? Assoc. Petrol. Geochem. Explor. Bull. 11, 1 –56.

Kusumastuti, A., Van Rensbergen, P., Warren, J.K., (2002) - Seismic sequence analysis and reservoir potential of drowned Miocene carbonate platforms in the Madura Strait, East Java, Indonesia. Aapg Bull. 86, 213–232.

Laske G. & Masters G., A Global Digital Map of Sediment Thickness, EOS Trans. AGU, 78, F483, 1997. https://igppweb.ucsd.edu/~gabi/sediment.html

Lazar J., Kanduč T., Jamnikar S., Grassa F., Zavšek S. (2014) - Distribution, composition and origin of coalbed gases in excavation fields from the Preloge and Pesje mining areas, Velenje Basin, Slovenia. International Journal of Coal Geology 131, 363–377.

Liu, Q., Dai, J., Jin, Z., Li, J., Wu, X., Meng, Q., Yang, C., Zhou, Q., Feng, Z., Zhu, D., 2016. Abnormal carbon and hydrogen isotopes of alkane gases from the Qingshen gas field, Songliao Basin, China, suggesting abiogenic alkanes? J. Asian Earth Sci.115, 285–297.

Lizarralde D., Axen G.J., Brown H.E., Fletcher J.M., Gonzalez-Fernandez A., Harding A.J., Holbrook W.S., Kent G.M., Param P., Sutherland F. and Umhoefer P.J. (2007) - Variation in styles of rifting in the Gulf of California. Nature, 448, doi:10.1038/nature06035.

Lonsdale, P., and K. Becker, 1985, Hydrothermal plumes, hot spots, and conductive heat flow in the southern trough of Guaymas basin: Earth and Planetary Science Letters, v. 73, p. 211-225.

Lowenstern J.B., Bergfeld D., Evans W.C., Hunt A.G. (2015) - Origins of geothermal gases at Yellowstone. Journal of Volcanology and Geothermal Research, doi: 10.1016/j.jvolgeores.2015.06.010

Lowenstern, J. B., D. Bergfeld, W. C. Evans, and S. Hurwitz (2012), Generation and evolution of hydrothermal fluids at Yellowstone: Insights from the Heart Lake Geyser Basin, Geochem. Geophys. Geosyst., 13, Q01017, doi:10.1029/2011GC003835.

Lowenstern J. B., Janik Cathy J., Fahlquist Lynne S., Johnson Linda S. (1999) - Gas and isotope geochemistry of 81 steam samples from wells in The Geysers geothermal field, Sonoma and Lake Counties, California, U.S.A. Open-File Report 99-304 Available online at: http://wrgis.wr.usgs.gov/open-file/of99-304/

Lu D. & Lin J.T. (1986) - Carbon and hydrogen isotopes of natural gas in western Taiwan. Petrol. Geol. Taiwan 22, 55-67.

Lupi, M., Saenger, E. H., Fuchs, F. & Miller, S. A. (2013) Lusi mud eruption triggered by geometric focusing of seismic waves. Nature Geosci. 6, 642–646.

Mazzini A., Svensen H. a, Akhmanov G.G., Aloisi G., Planke S., Malthe-Sørenssen A., Istadi B. (2007) Triggering and dynamic evolution of the LUSI mud volcano, Indonesia. Earth and Planetary Science Letters. Volume 261, Issues 3–4

Mazzini, A., Svensen H., Etiope G., Onderdonk N., and Banks D. (2011), Fluid origin, gas fluxes and plumbing system in the sediment-hosted Salton Sea Geothermal System (California, USA), J. Volcanol. Geotherm. Res., 205, 76–83.

Mazzini A., Etiope G., Svensen H., (2012) A new hydrothermal scenario for the 2006 Lusi eruption, Indonesia. Insights from gas geochemistry. Earth and Planetary Science Letters, 317–318, 305–318.

Mazzini A. and the Lusi Lab team (2017) The Lusi eruption site: insights from surface and subsurface investigations. American Geophysical Union Fall Meeting, 2017. ID# 27695

Mazzini A. & Etiope G., (2017) - Mud volcanism: An updated review. Earth Science Reviews, doi: 10.1016/j.earscirev.2017.03.001

Mazzini, A., Scholz, F., Svensen, H. H., Hensen, C., and Hadi, S., 2018, The geochemistry and origin of the hydrothermal water erupted at Lusi, Indonesia: Marine and Petroleum Geology, v. 90, p. 52-66.

Merril M. D., Hunt A.G. & Lohr C.D., (2014) - Noble gas geochemistry investigation of high $_{CO2}$ natural gas at the LaBarge Platform, Wyoming, USA. Energy Procedia 63, 4186 – 4190.

Mi, J., Zhang, S., Hu, G., He, K., 2010. Geochemistry of coal-measure source rocks and natural gases in deep formations in Songliao Basin, NE China. Int. J. Coal Geol.84, 276–285.

Milkov AV., Etiope G. (2018) - Geochemistry of Shale Gases from around the World. 80th EAGE Conference and Exhibition 2018.

Mörner, N. A., and G. Etiope (2002), Carbon degassing from the lithosphere, Global Planet. Change, 33, 185–203

Nicholson K.N. (1993) - Geothermal Fluids. Chemistry and Exploration Techniques. Ed. Springer-Verlag, 263 pp., ISBN 3 540 56017 3.

Northern Petroleum (2002) - Relazione geologica, Istanza permesso di ricerca Fiume Tevere, in Progetto VIDEPI, Ministero dello Sviluppo Economico, DGRME, Società Geologica Italiana and Assomineraria, Northern Petroleum. [Available at www.unmig.sviluppoeconomico. gov.it/videpi.]

Onderdonk, N., Mazzini, A., Shafer, L., and Svensen, H., 2011, Controls on the geomorphic expression and evolution of gryphons, pools, and caldera features at hydrothermal seeps in the Salton Sea Geothermal Field, southern California: Geomorphology, v. 130, p. 327-342.

Palcsu L., Vető I., Futó I., Vodila G., Papp L., Major Z. (2014) - In-reservoir mixing of mantle-derived CO_2 and metasedimentary CH_4-N_2 fluids e Noble gas and stable isotope study of two multistacked fields (Pannonian Basin System, W-Hungary). Marine and Petroleum Geology 54, 216-227.

Pallasser, R.J., 2000. Recognising biodegradation in gas/oil accumulations through the delta C-13 compositions of gas components. Org. Geochem. 31, 1363-1373.

Polozov, A.G., Svensen, H.H., Planke, S., Grishina, S.N., Fristad, K.E., Jerram, D.A., 2016. The basalt pipes of the Tunguska Basin (Siberia, Russia): high temperature processes and volatile degassing into the end-Permian atmosphere. Palaeogeogr. Palaeoclimatol. Palaeoecol. 441, 51–64.

Queißer M., Burton M. R., Arzilli F., Chiarugi A., Indah Marliyani G., Anggara F. and Harijoko A. (2017) - CO_2 flux from Javanese mud volcanism. doi: 10.1002/2017JB013968

Päivi L., Ketil J., Thieme R. & Thieme N. (2007) - 'Fighting over Oil: Introducing A New Dataset', *Conflict Management and Peace Science* 24(3), 239-256.

Porro C. and Augustine C. (2012) - Estimate of Geothermal Energy Resource in Major U.S. Sedimentary Basins. National Renewable Energy Lab presentation.

Reynolds, P., Planke, S., Millett, J. M., Jerram, D. A., Trulsvik, M., Schofield, N., and Myklebust, R., 2017, Hydrothermal vent complexes offshore Northeast Greenland: A potential role in driving the PETM: Earth and Planetary Science Letters, 467, 72-78.

Robertson Basins and Plays (Tellus TM) - Sedimentary Basins of the World Map. http://www.datapages.com/gis-map-publishing-program/gis-open-files/global-framework/robertson-tellus-sedimentary-basins-of-the-world-map. (Last download April 2018)

Rybach L. (1981) - Geothermal systems, conductive heat flow, geothermal anomalies. L. Rybach, LJP Muffler (Eds.), Geothermal systems: Principles and case histories, John Wiley & Sons, ChichesterUK, pp. 3-31.

Satyana A.H. (2008) - Mud diapirs and mud volcanoes in depressions of Java to Madura: origins, natures, and implications to petroleum system. IPA 32nd Annual Convention Proceedings, IPA08-G-139, 1-34.

Schoell M., (1988) – Multiple origins of methane in the earth. Chemical geology, 71, 1-10.

Schwietzke S., Sherwood O.A., Bruhwiler L.M.P., Miller J.B., Etiope G., Dlugokencky E. J., Englund Michel S., Arling V. A., Vaughn B. H., White J. W. C. & Tans P. P. (2016) - Upward revision of global fossil fuel methane emissions based on isotope database. 8 8 | Nature, 538, doi:10.1038/nature19797.

Scrocca D., Doglioni C., Innocenti F. (2003) - Contraints for an interpretation of the italian geodynamics: a review. Mem. Descr. Carta Geol. d'It. LXII, 15-46.

Sella P., P., Billi A., Mazzini I., De Filippis L., Pizzino L., Sciarra A., and Quattrocchi F. (2014), A newly-emerged (August 2013) artificially triggered fumarole near the Fiumicino airport, Rome, Italy, J. Volcanol. Geotherm. Res., 280, 53–66.

Shuai Y., Etiope G., Zhang S., Douglas P.M.J., Huang L., Eiler J.M. (2018) – Methane clumped isotopes in the Songliao Basin (China): New insights into abiotic vs. biotic hydrocarbon formation. Earth and Planetary Science Letters, 482, 213-221.

Sherwood, O.A., Schwietzke, S., Arling, V.A., Etiope, G., 2017. Global inventory of gas geochemistry data from fossil fuel, microbial and biomass burning sources, version 2017. Earth Syst. Sci. Data9, 639–656. https://doi.org/10.5194/essd-9-639-2017.

Simoenit B.R.T. & Galimov E.M. (1984) Geochemistry of interstitial gases in quaternary sediments of the Gulf of California. Chemical Geology, 43, 151-166

Simoneit B.R.T. (1988) Petroleum generation in submarine hydrothermal systems: an update. Canadian Mineralogist 26, 827-840.

Smith J.W., Gould K.W. and Rigby D. (1982) – The stable isotope geochemistry of Australian coals. Org. Geochem., 3, 111-131.

Sun C.H., Chang S.C., Kuo C.L., Wu J.C., Shao P.-H., Oung J.-N. (2010) - Origins of Taiwan's mud volcanoes: Evidence from geochemistry. Journal of Asian Earth Sciences 37, 105–116

Svensen, H., S. Planke, B. Jamtveit, and T. Pedersen (2003), Seep carbonate formation controlled by hydrothermal vent complexes: A case study from the Voring Basin, the Norwegian Sea, Geo Mar. Lett., 23, 351 –358, doi:10.1007/s00367-003-0141-2.

Svensen, H., S. Planke, A. Malthe-Sorenssen, B. Jamtveit, R. Myklebust, T. R. Eidem, and S. S. Rey (2004), Release of methane from a volcanic basin as a mechanism for initial Eocene global warming. Nature, 429, 542–545.

Svensen, H., D. A. Karlsen, A. Sturz, K. Backer-Owe, D. A. Banks, and S. Planke (2007), Processes controlling water and hydrocarbon composition in seeps from the Salton Sea geothermal system, California, USA, Geology, 35, 85– 88, doi:10.1130/G23101A.1.

Svensen, H., Planke, S., Chevallier, L., Malthe-Sørenssen, A., Corfu, F., and Jamtveit, B., 2007, Hydrothermal venting of greenhouse gases triggering Early Jurassic global warming: Earth and Planetary Science Letters, 256, 554–566, doi:10.1016/j.epsl.2007.02.013.

Svensen, H., Planke, S., Polozov, A.G., Schmidbauer, N., Corfu, F., Podladchikov, Y.Y., and Jamtveit, B., 2009, Siberian gas venting and the end- Permian environmental crisis: Earth and Planetary Science Letters, 277, 490–500, doi:10.1016/j.epsl.2008.11.015

Svensen H., Hammer Ø., Mazzini A., Onderdonk N., Polteau S., Planke S., and Podladchikov Y. Y. (2009) Dynamics of hydrothermal seeps from the Salton Sea geothermal system (California, USA) constrained by temperature monitoring and time series analysis. Journal of Geophysical Research, vol. 114, b09201, doi:10.1029/2008jb006247

Svensen, H., Polteau, S., Cawthorn, G., Planke, S., 2015. Sub-volcanic intrusions in the Karoo Bains, South Africa. Advances in volcanology http://dx.doi.org/10.1007/11157_2014_7 (in press).

Tanikawa Wataru, Sakaguchi Masumi, Teguh Wibowo Handoko, Shimamoto Toshihiko, Tadai Osamu (2010) Fluid transport properties and estimation of overpressure at the Lusi mud volcano, East Java Basin. Engineering Geology 116, 73–85.

Taran Y.A., Giggenbach W. F. (2003) - Geochemistry of Light Hydrocarbons in Subduction-Related Volcanic and Hydrothermal Fluids. Society of Economic Geologists Special Publication 10, p. 61–74, Chapter 6.

Tassi F., Montegrossi G., Capecchiacci F & Vaselli O., (2010) - Origin and Distribution of Thiophenes and Furans in Gas Discharges from Active Volcanoes and Geothermal Systems. Int. J. Mol. Sci., 11, 1434-1457; doi:10.3390/ijms11041434.

Tassi F., Fiebig J., Vaselli O., Nocentini M., (2012) - Origins of methane discharging from volcanic-hydrothermal, geothermal and cold emissions in Italy. Chemical Geology 310–311, 36–48.

Teske A., de Beer D., McKay L.J., Tivey M.K., Biddle J.F., Hoer D., Lloyd Karen G., Lever M.A., Røy H., Albert D.B., Mendlovitz H.P. and MacGregor B.J. (2016) - The Guaymas Basin Hiking Guide to Hydrothermal Mounds, Chimneys, and Microbial Mats: Complex Seafloor Expressions of Subsurface Hydrothermal Circulation. Front. Microbiol. 7:75. doi:

Von Damm K. L., Edmond J. M., Measures C. I. and Grant B. (1985) - Chemistry of submarine hydrothermal solutions at Guaymas Basin, Gulf of California. Geochimica et Cosmochimica Acta, 49, 2221-2237.

Wang, X., Guo, Z., Tuo, J., Guo, H., Li, Z., Zhuo, S., Jiang, H., Zeng, L., Zhang, M., Wang, L., 2009. Abiogenic hydrocarbons in commercial gases from the Songliao Basin, China. Sci. China, Ser. D52, 213–226.

Wang P.J., Mattern F., Didenko N.A., Zhu D.F., Singer B., Sun X.M (2016) – Tectonics and cycle system of the Cretaceous Songliao Basin: An inverted active continental margin basin. Earth-Science Reviews 159, 82–102

Welhan J.A. & Lupton J.E. (1987) Light hydrocarbon gases in Guaymas Basin hydrothermal fluids: thermogenic versus abiogenic origin. The American Association of Petroleum Geologist Bulletin, 71, 215-223.

Welhan J.A. (1988) Origins of methane in hydrothermal systems. Chemical Geology, 71, 183-198.

Whiticar, M. J. (1999), Carbon and hydrogen isotope systematics of bacterial formation and oxidation of methane, Chem. Geol., 161, 291–314.

Younker, L.W., Kasameyer, P.W., Tewhey, J.D., (1982) - Geological, Geophysical, and Thermal characteristics of the Salton Sea Geothermal Field, California, Journal of Volcanology and Geothermal Research, 12; pp. 221-258, 1982.

Figure captions

Figure 1: Sketch of the sequence of SHGS identification criteria. Examining CO_2-rich systems known in the literature, the peculiar gas-geochemical characteristics (isotopic and molecular) of previously recognized SHGSs, have been used as a first diagnostic tool to identify new SHGSs. Statistical and spatial analysis of geological data related to the new SHGSs, including heat-flow, sediment thickness and geographic distances from volcanic centers and petroleum fields, has allowed to map additional, potential SHGS areas in all continents.

Figure 2. Location and simplified cross-sections (not to scale) of the previously identified SHGSs. (a) Guaymas Basin (modified after Lizarralde et al., 2007) (b) Salton Sea (modified after Bennett, 2011); (c) Lusi (modified after Satyana, 2008). (d) Tiber Delta-Fiumicino SHGS (modified after Carminati and Doglioni 2012). (e) Songliao Basin **(**modified after Wang et al., 2016), HTB: Hai Tan Basin, Tanlu G-H-R: Graben and horst range of the northern Tanlu Strike-Slip Fault System, SA Belt: Sikhote-Alin Orogenic Belt.

Figure 3. Normal Probability Plots (NPP) of methane concentration (a) and $\delta^{13}C$-CH_4 (b) in SHGS, volcanoes and conventional geothermal systems. The deviation from a normal distribution is recorded at 1.5 vol.% and around -30 ‰, respectively.

Figure 4. Conceptual sketch of a SHGS (hybrid system) and relationship with the endmembers, volcano-geothermal and hydrocarbon systems. The sketch is not to scale.

Figure 5: Global distribution of the newly identified SHGSs (brown dots) in North America (a), Europe (b) and, Eastern Asia and Oceania (c). Black dots refer to SHGSs identified in previous works. Numbers refer to Table 2.

Figure 6: Gas molecular and isotopic geochemical diagrams of CO_2 and CH_4 in SHGSs and comparison with volcano, conventional geothermal (CGS) and hydrocarbon systems. Volcanic-geothermal data are described in *Supplementary Material*. Hydrocarbon gas data are from Sherwood et al. (2017) and CGG (2015). a) CH_4 vs CO_2 concentration. Some CGSs and volcanoes have relatively high CH_4 concentrations (> 1.5 vol.%, dashed line), these samples lack isotopic data or have $\delta^{13}C$-CH_4 values higher than the SHGS threshold (-30 ‰, see diagram 6b) so that the SHGS attribution is not possible at this stage. b) $\delta^{13}C$-CH_4 vs CH_4 concentration; c) $\delta^{13}C$-CO_2 vs CO_2 concentration; isotopic CO_2 genetic fields are from Jenden et al., (1988) and Etiope et al., (2009). Tm thermomethamorphism; M-M magma-mantle degassing; SM secondary methanogenesis; OB oil biodegradation; O organic; d) $\delta^{13}C$-CH_4 vs $\delta^{2}H$-CH_4 (redrawn after Etiope, 2017). M microbial; T thermogenic; A abiotic; MCR microbial carbonate reduction; MAF microbial acetate fermentation; ME microbial in evaporitic environment; T_H thermogenic high maturity; T_{LM} thermogenic low maturity; GM geothermal and magmatic; S serpentinized rocks; PC Precambrian shields. The legend is the same for all diagrams, the green areas in diagrams *a*, *b* and *c* are relative to hydrocarbon systems.

Figure 7: Multiple Correspondence diagram among the variable a) HF heat flow; b) ST Sediment thickness; c) dV distance from nearest volcano; d) dH distance from nearest hydrocarbon field. Code "0" and "1" are relative to values (rounded-up) outside and within the 95% confidence limit, respectively (see Tab. 4). In particular, for a) and b) the range values were considered, whereas for the variables c) and d) the maximum confidence limit values were considered. The light orange area shows the correlation among the variables a), c) and d).

Figure 8: Workflow relative to the mapping of SHGS prone areas. Top: input raster dataset; Bottom: resulting global map. The location of palaeo-SHGS is from Svensen et al., 2003; Svensen et al., 2015; Jones et al., 2016; Jamtveit et al., 2004.

Figure 9: SHGS conceptual geological sketch (introduced in figure 4) integrated with geological and geochemical parametrization resulting from the present study. In particular, the main gas-geochemical features are summarised for the SHGSs (hybrid system) and for the endmembers, volcano-geothermal and hydrocarbon systems. Related CO_2 and CH_4 genetic processes are also specified (from Etiope and Sherwood, 2013). The sketch is not to scale.

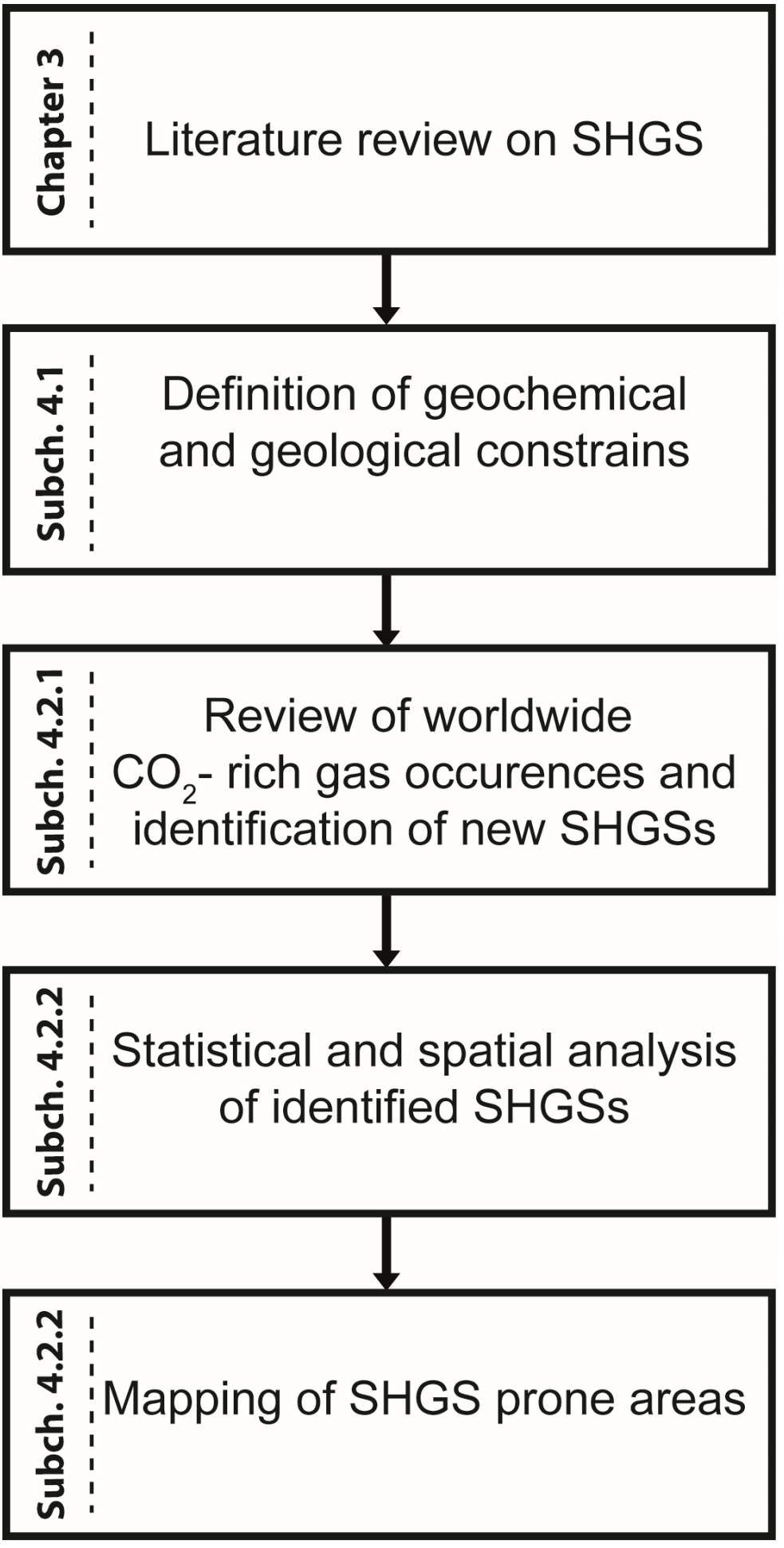
Chapter 3
Literature review on SHGS
Subch. 4.1
Definition of geochemical and geological constrains
Subch. 4.2.1
Review of worldwide CO_2- rich gas occurences and identification of new SHGSs
Subch. 4.2.2
Statistical and spatial analysis of identified SHGSs
Subch. 4.2.2
Mapping of SHGS prone areas

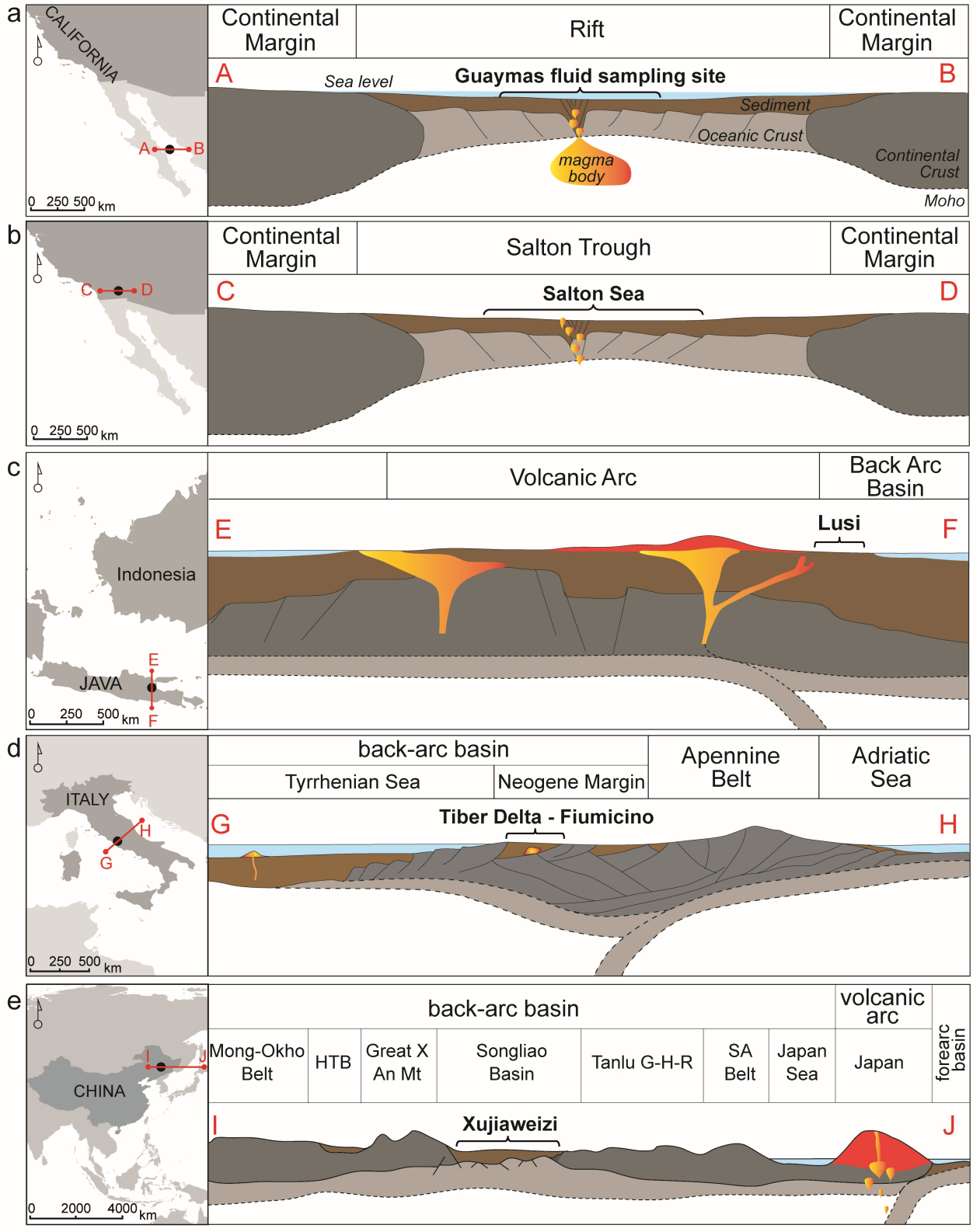
a
CALIFORNIA
A
B
0 250 500 km
Continental Margin
Rift
Continental Margin
A
Sea level
Guaymas fluid sampling site
B
Sediment
Oceanic Crust
magma body
Continental Crust
Moho
b
C
D
0 250 500 km
Continental Margin
Salton Trough
Continental Margin
C
Salton Sea
D
c
Indonesia
JAVA
E
F
0 250 500 km
Volcanic Arc
Back Arc Basin
E
Lusi
F
d
ITALY
H
G
0 250 500 km
back-arc basin
Tyrrhenian Sea
Neogene Margin
Apennine Belt
Adriatic Sea
G
Tiber Delta - Fiumicino
H
e
CHINA
I
J
0 2000 4000 km
back-arc basin
volcanic arc
Mong-Okho Belt
HTB
Great X An Mt
Songliao Basin
Tanlu G-H-R
SA Belt
Japan Sea
Japan
forearc basin
I
Xujiaweizi
J

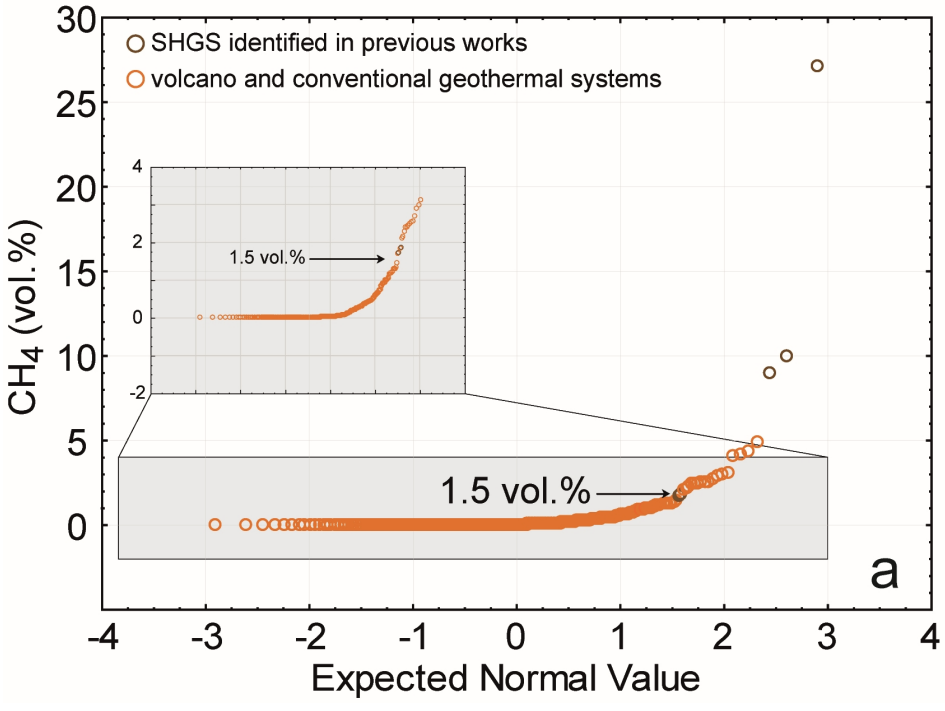
SHGS identified in previous works
volcano and conventional geothermal systems
CH4 (vol.%)
1.5 vol.%
1.5 vol.%
a
Expected Normal Value

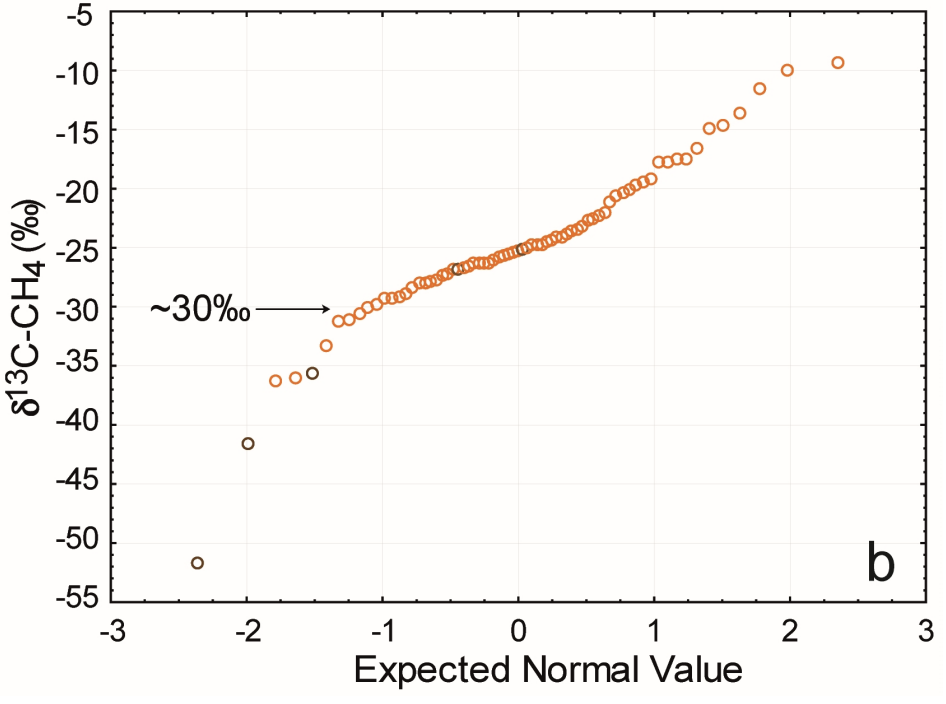
δ13C-CH4 (‰)
~30‰
b
Expected Normal Value

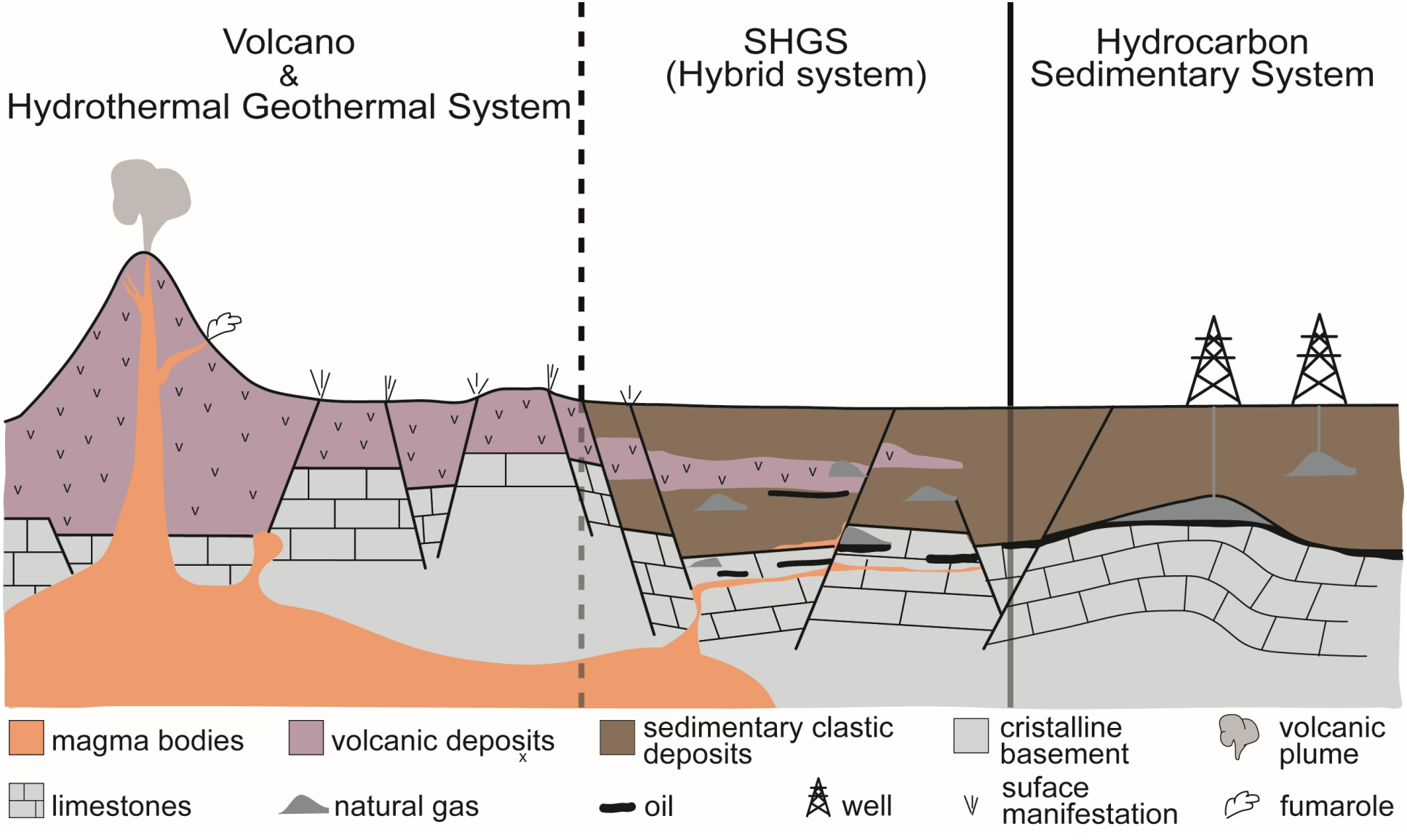
Volcano
&
Hydrothermal Geothermal System
SHGS
(Hybrid system)
Hydrocarbon
Sedimentary System
magma bodies
volcanic deposits
sedimentary clastic deposits
cristalline basement
volcanic plume
limestones
natural gas
oil
well
suface manifestation
fumarole

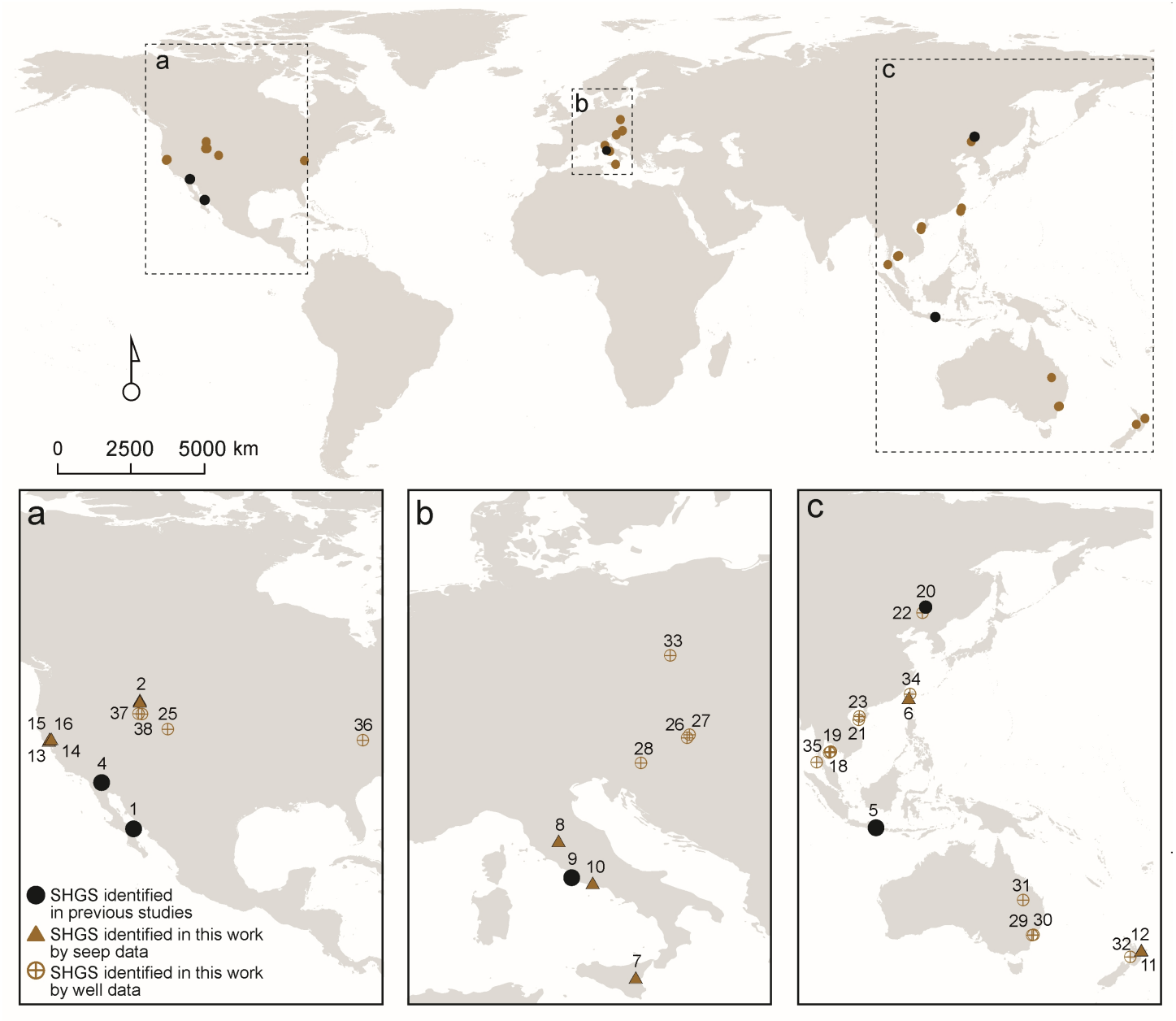
a
b
c
0 2500 5000 km
a
b
c
SHGS identified in previous studies
SHGS identified in this work by seep data
SHGS identified in this work by well data
1
2
4
5
6
7
8
9
10
11
12
13
14
15
16
18
19
20
21
22
23
25
26
27
28
29
30
31
32
33
34
35
36
37
38

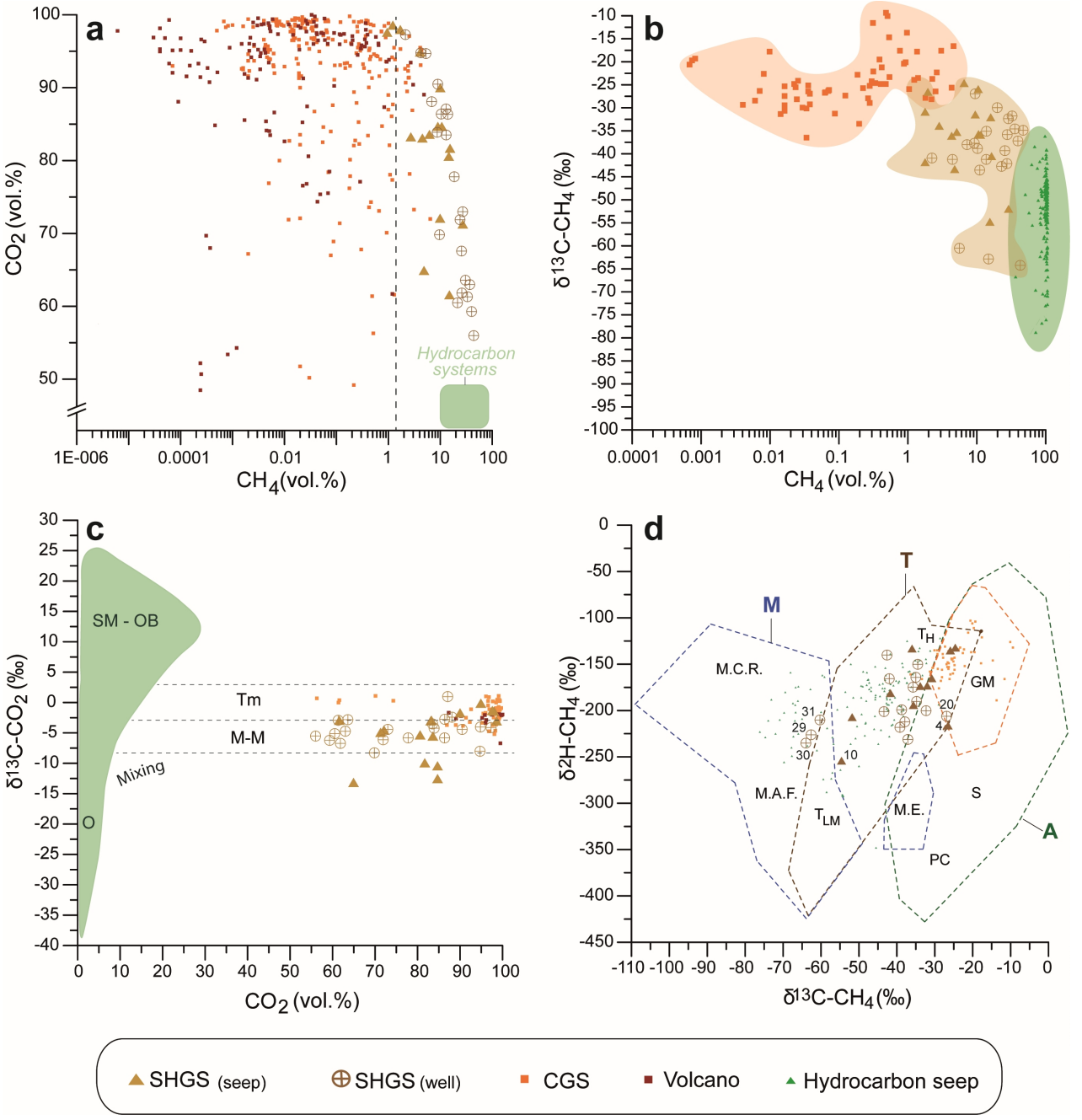
a
CO2 (vol.%)
CH4(vol.%)
Hydrocarbon systems
b
δ13C-CH4 (‰)
CH4 (vol.%)
c
δ13C-CO2 (‰)
CO2 (vol.%)
SM - OB
Tm
M-M
Mixing
O
d
δ2H-CH4 (‰)
δ13C-CH4 (‰)
M
T
A
S
GM
PC
M.C.R.
M.A.F.
M.E.
TH
TLM
SHGS (seep)
SHGS (well)
CGS
Volcano
Hydrocarbon seep

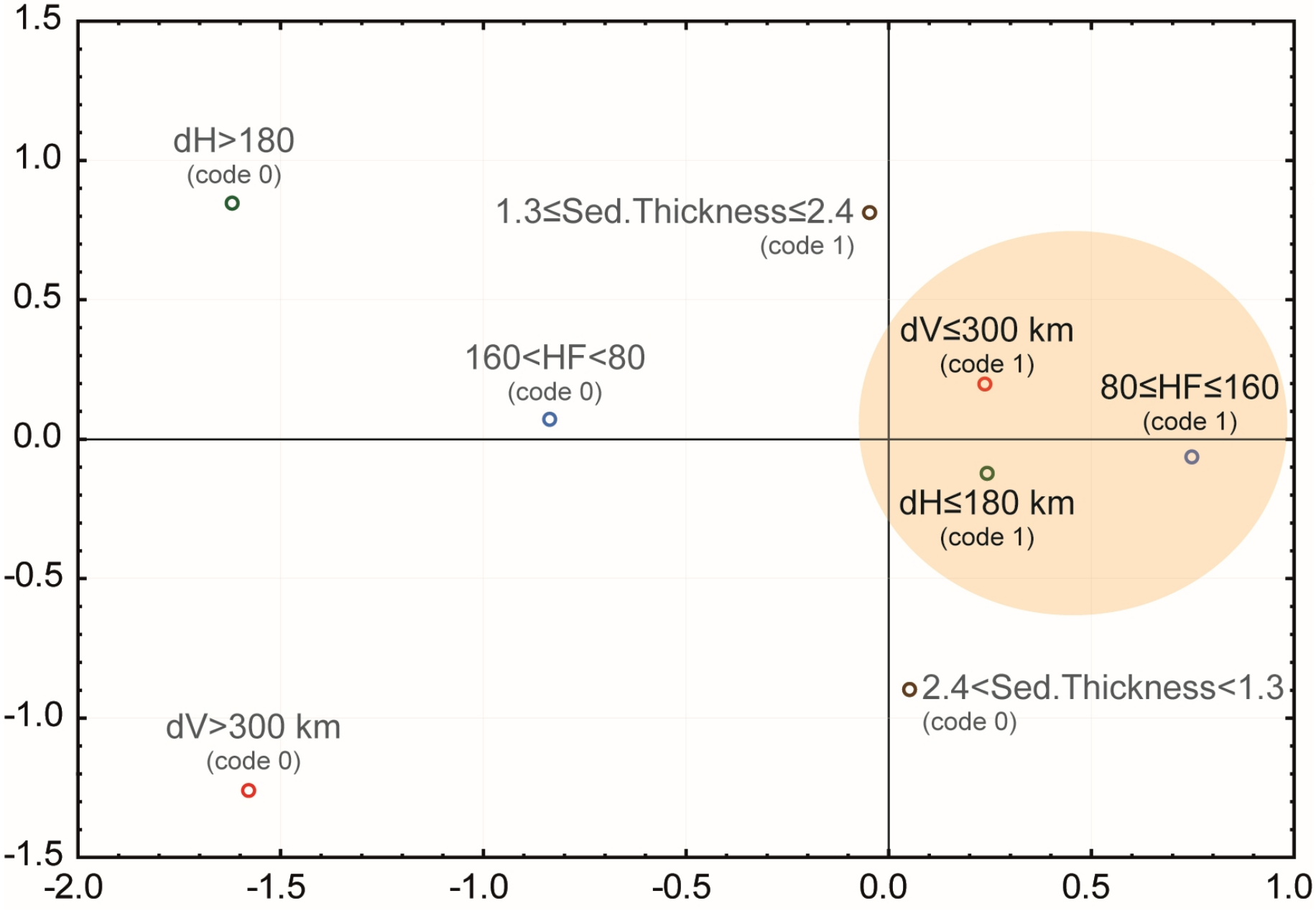
1.5
1.0
0.5
0.0
-0.5
-1.0
-1.5
-2.0
-1.5
-1.0
-0.5
0.0
0.5
1.0
dH>180
(code 0)
1.3≤Sed.Thickness≤2.4
(code 1)
dV≤300 km
(code 1)
160<HF<80
(code 0)
80≤HF≤160
(code 1)
dH≤180 km
(code 1)
2.4<Sed.Thickness<1.3
(code 0)
dV>300 km
(code 0)

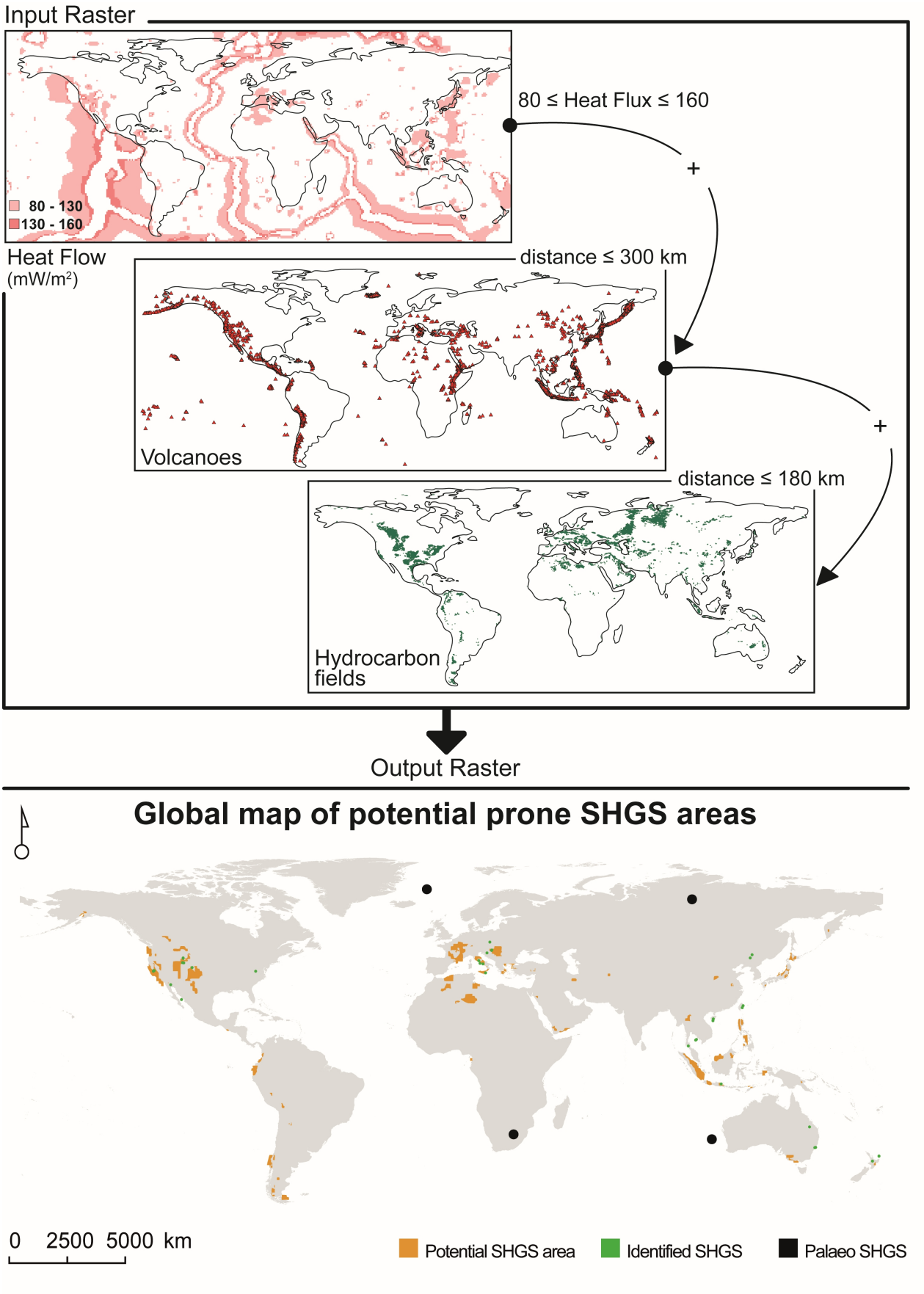
Input Raster
80 - 130
130 - 160
Heat Flow
(mW/m²)
80 ≤ Heat Flux ≤ 160
+
distance ≤ 300 km
Volcanoes
+
distance ≤ 180 km
Hydrocarbon fields
Output Raster
Global map of potential prone SHGS areas
0 2500 5000 km
Potential SHGS area
Identified SHGS
Palaeo SHGS

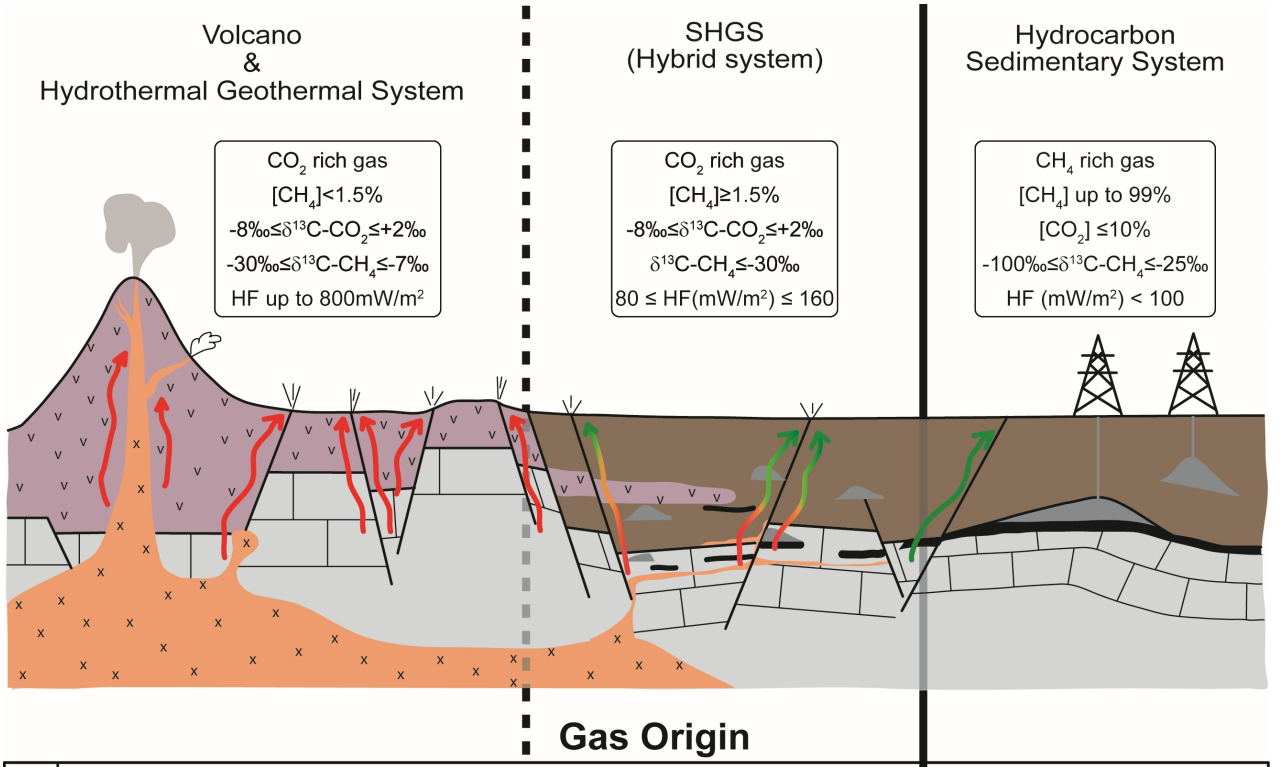

Gas Origin

CO_2	**inorganic**	**organic**
	Magma-mantle degassing and thermometamorphism reactions	Thermogenesis (e.g. kerogene decarboxilation)
CH_4	**abiotic**	**biotic**
		Thermogenic / ***Microbial***
	Magmatic and post-magmatic high T reaction	Thermal cracking of organic matter (catagenesis) or oil at high T (70-250°C) / Diagenesis of sediments (up to 60–80 °C)

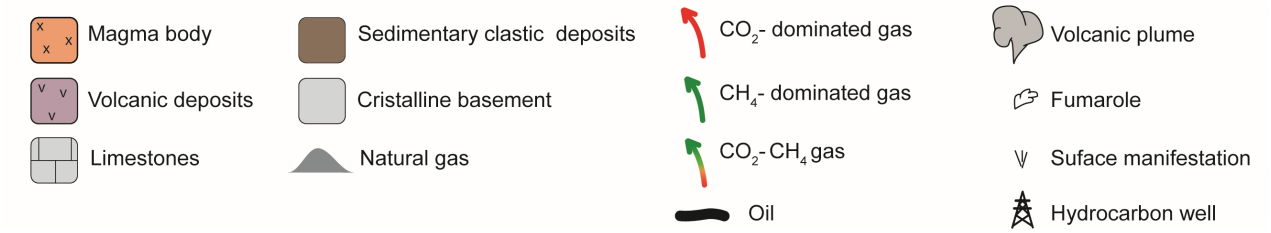

SITE	COUNTRY	DOMAIN	GAS DISCHARGE						BASIN		OIL TRACE/ GAS FIELD	HEAT FLUX (mW/m^2)	REFERENCE
			Type	CO_2 vol.%	CH_4 vol.%	$\delta^{13}C\text{-}CO_2$ ‰	$\delta^{13}C\text{-}CH_4$ ‰	$\delta^{2}H\text{-}CH_4$ ‰	Thickness Sediment (km)	Main lithology			
Tiber-Delta	Italy	back arc basin	bp	98*	1.0* up to 1.7	-2.1 ÷ -0.7	-54.1 ÷ -37	-205÷ -162	2	Limestones to clay-sandstones	✓	100 ÷ 250	[1-4]
Salton Sea	California	pull-apart basin	bp+v+g	99*	1.2* up to 1.9	-5.4 ÷ 0.2	-32.7 ÷ -17.6	-270 ÷ -150	0.7÷ 4	carbonate	✓	up to 600	[5, 6]
Guaymas Basin	Gulf of California	rift	sv	~90	~10	-6 ÷ 2.7	-50.8 ÷ -43.2	-265 ÷ -123	0.7÷ 1	diatomaceous calcareous	✓	up to 453	[7-9]
Lusi	Indonesia	back arc basin	bp+v	71* up to 99	27.1* up to 35	-12.8 ÷ -2.2	-51.8÷ -31	-207	2÷ 4	clay volcanoclastic-sand, limestone	✓	60 ÷ 100	[10-12]
Songliao Basin	China	retro-arc basin	well	90.5	8.94	-4.4	-26.9	-206	1÷5	volcanic rocks	✓	50 ÷ 100	[13]

Tab.1*: Features of the SHGSs characterized in previous works. bp: bubbling pool; v: vent; sv: submarine vent; g: gryphon. * mean value; [1] Ciotoli et al., 2016; [2] Carapezza et al., 2015; [3] Della Vedova et al., 2001; [4]* Northern Petroleum (2002); [5] *Mazzini et al., 2011; [6] Younker et. al.,1982; [7] Simoneit & Galimov, 1984; [8] Welhan, 1987; [9] Welhan, 1988; [10] Mazzini et al., 2012; [11] Mazzini & Lusi Lab Team, 2017; [12] Tanikawa et al., 2010; [13] Shuai et al., 2018.*

ID	LOCATION	COUNTRY/STATE	TYPE	CO_2	N_2	CH_4	CH_{4max}	C_{2+}	H_2	H_2S	He	R/Ra©	$\delta^{13}C$-CO_2	$\delta^{13}C$-CH_4	$\delta^{2}H$-CH_4	Reference
1*	Guaymas Basin	California	v	90.0	-	10.00	-	-	-	-	-	-	-1.7	-35.6	-194	[1, 2]
2	Heart Lake	Wyoming	v	83.1	10.500	4.53	-	0.015	0.023	0.660	0.067	1.1	-3.0	-43.2	-	[3]
3	Johnson Spring	Wyoming	bp	83.3	12.850	2.71	-	-	-	-	-	0.1	-2.9	-33.8	-173	[4]
4*	Salton Sea	California	bp	98.1	-	1.86	-	0.03	-	-	-	6.5	-1.6	-26.5	-216	[5]
5*	Lusi Crater	Indonesia	bp	73.3	-	24.92	39.85	1.449	-	-	-	5.5	-3	-51.8	-207	[6, 7]
6	Chukou Fault	Taiwan	bp	61.6	-	15.00	33.60	0.290	-	-	-	-	-2.9	-32.0	-173	[8]
7	Salinelle Paternò	Italy	bp	94.9	0.900	4.10	-	0.004	-	-	-	6.5	-0.4	-36.0	-133	[9-11]
8	Torrite di Siena	Italy	bp	98.0	0.330	1.70	-	0.009	-	-	-	-	-1.4	-30.8	-165	[10]
9*	Fiumicino	Italy	bp	98.3	-	1.70	-	0.001	-	-	-	0.2	-1.3	-41.7	-181	[12-14]
10	Laghi del Vescovo	Italy	bp	80.6	4.700	14.60	-	0.002	-	0.016	-	-	-5.3	-54.6	-254	[10]
11	Calypso North	New Zealand	v	83.6	9.370	6.20	-	0.006	-	0.820	-	-	-5.5	-24.6	-132	[15]
12	Calypso North	New Zealand	v	72.1	16.920	9.90	-	0.074	-	1.030	-	-	-4.5	-25.9	-135	[15]
13	The Geysers	Northern California	v	64.9	11.484	4.86	9.39	-	11.860	3.879	0.002	-	-13.1	-35.2	-	[16]
14	Clear Lake	Northern California	v	84.7	-	8.98	53.00	-	-	-	-	-	-12.5	-31.4	-	[17]
15	Sulphur Bank	Northern California	v	84.7	-	10.70	18.20	-	-	-	-	-	-10.4	-35.8	-	[17]
16	Wilbur Spring	Northern California	v	81.7	-	15.40	49.90	-	-	-	-	-	-9.9	-40.4	-	[17]
17	Gulf of Thailand	Thailand	w	55.0	-	43.00	-	2.000	-	-	-	-	-5.5	-34.8	-190	[18]
18	Gulf of Thailand	Thailand	w	63.0	-	33.00	-	4.000	-	-	-	-	-4.7	-37.1	-231	[18]
19	Gulf of Thailand	Thailand	w	71.0	-	27.00	-	2.000	-	-	-	0.18	-4.4	-32.3	-200	[18]
20*	Songliao Basin	China	w	90.5	0.450	8.94	-	0.090	-	-	-	2.2	-4.4	-26.9	-206	[19]
21	Yingqiong Basin	China	w	83.9	6.600	8.70	-	0.700	-	-	-	-	-4.2	-37.6	-	[20]
22	Changling Basin	China	w	77.8	3.200	18.60	-	0.440	-	-	-	-	-5.8	-29.9	-	[20]
23	Dongfang	China	w	63.6	4.700	30.50	-	1.200	-	-	-	-	-2.8	-31.7	-	[20]
24	Sheep Mountain	Colorado	w	97.3	0.666	2.13	-	-	-	-	-	-	-4.1	-40.8	-	[21]
25	Sheep Mountain	Colorado	w	94.8	1.540	4.21	-	-	-	-	-	-	-4.0	-41.1	-	[21]
26	Pannonian System	Hungary	w	88.1	5.090	6.82	-	-	-	-	-	-	-2.4	-37.9	-212	[22]
27	Pannonian System	Hungary	w	86.4	2.870	10.40	-	-	-	-	-	-	-2.7	-43.4	-201	[22]
28	Velenje Basin	Slovenia	w	87.1	-	12.90	-	-	-	-	-	-	1.0	-41.1	0.0	[23]
29	Colliery	Australia	w	86.4	-	13.93	19.80	0.040	-		-	-	-5.8	-62.6	-226	[24, 25]
30	Darkes Forest	Australia	w	59.3	-	40.00	--	-	-	-	-	-	-6.2	-64.0	-235	[24, 25]
31	Collinsville	Australia	w	94.7	-	5.30	-	0.050	-	-	-	-	-8.0	-60.3	-210	[24, 25]
32	Taranaki	New Zealand	w	67.6	3.950	25.70	35.00	1.350	-	-	-	-	-0.3	-42.0	-166	[25-27]
33	Walbrzych coal basin	Poland	w	69.8	18.560	9.66	15.50	1.426	-	-	-	-	-8.3	-38.7	-199	[25, 28]
34	Chiayi-Yunshui	Taiwan	w	61.8	11.613	25.97	44.28	0.363	-	-		-	-6.7	-35.7	-174.7	[25, 29]
35	Platong	Thailand	w	71.9	0.880	24.00	-	3.561	0.009	-	0.002	-	-6.1	-39.2	-218.0	[25, 30]
36	Wildcat	West Virginia	w	83.5	2.230	13.00	-	0.124	0.005	-	0.106	-	-3.5	-35.0	-164.0	[30]
37	Indian creek	Wyoming	w	61.3	2.730	33.40	-	0.260	-	-	0.114	-	-2.9	-34.5	-150.0	[30]
38	Labarge platform	Wyoming	w	60.5	7.710	21.50	-	0.015	4.005	-	0.592	-	-5.1	-42.7	-140.0	[25, 30]

Tab.2: Molecular and isotopic composition of the gas related to SHGS suggested in this work. Gas composition is in vol.%. Isotopic data: $\delta^{13}C$: ‰ VPDB; $\delta^{2}H$: ‰ VSMOW; R/Ra_c = ($^{3}He/^{4}He$)sample/($^{3}He/^{4}He$)atmosphere; Ra= 1.39 x 10^{-6}. Sediment thickness in km. Heat Flux in mW/m^2. Hyphen: no data. Type: v= vent; bp= bubbling pool; w: well. For the molecular composition mean values are reported for the sites: 5, 6, 7, 13, 14, 15, 16, 29, 32, 33, 34, 38. Asterisk is for SHGSs recognized in previous works and discussed in chapter 3. [1] Welhan & Lupton, 1987; [2] Welhan, 1988; [3] Lowenstern et al., 2015; [4] Merril et al., 2014; [5] Mazzini et al., 2011; [6] Mazzini et al., 2012; [7] Mazzini & Lusi Lab Team, 2017; [8] Sun et al., 2010; [9] Grassa et al., 2004; [10] Tassi et al., 2012 ; [11] Caracausi et al., 2003; [12] Ciotoli et al., 2013 ; [13] Sella et al., 2014; [14] Carapezza et al., 2015 ; [15] Botz et al., 2002; [16] Lowenstern et al., 1999; [17] Bergfeld et al., 2001; [18] Giggenbach et al., 1997; [19] Shuai et al, 2018; [20] Dai et al., 2009; [21] Jenden et al., 1993; [22] Palcsu et al., 2014; [23] Lazar et al., 2014; [24] Smith et al., 1982; [25] Sherwood et al., 2017; [26] Giggenbach et al., 1997; [27] Hulston et al., 2001; [28] Kotarba & Rice, 2001; 29] Lu & Lin, 1986; [30] Jenden et al., 1988.

ID	LOCATION	COUNTRY	TYPE	Heat Flux (a)	Sediment thickness (b)	Distance from volcanoes (c)	Distance from hydrocarbon fields (d)
1*	Guaymas Basin	California	v	453	0.7	77	652
2	Heart Lake	Wyoming	v	487	1.4	22	42
3	Johnson Spring	Wyoming	bp	487	1.4	38	39
4*	Salton Sea	California	bp	118	1	4	193
5*	Lusi Crater	Indonesia	bp	73	2.3	11	0
6	Chukou Fault	Taiwan	bp	67	0.6	117	0
7	Salinelle Paternò	Italy	bp	103	5.5	18	0
8	Torrite di Siena	Italy	bp	103	1.3	29	40
9*	Fiumicino	Italy	bp	216	2	28	49
10	Laghi del Vescovo	Italy	bp	148	3.4	22	1
11	Calypso North	New Zealand	v	78	0.3	71	241
12	Calypso North	New Zealand	v	78	0.3	68	240
13	The Geysers	Northern California	v	100	1.7	17	54
14	Clear Lake	Northern California	v	100	1.7	13	41
15	Sulphur Bank	Northern California	v	78	1.1	10	44
16	Wilbur Spring	Northern California	v	78	1.1	32	23
17	Gulf of Thailand	Thailand	w	68	4.5	215	326
18	Gulf of Thailand	Thailand	w	68	5.9	200	325
19	Gulf of Thailand	Thailand	w	68	4.7	182	320
20*	Songliao Basin	China	w	65	5	316	154
21	Yingqiong Basin	China	w	73	4.3	160	156
22	Changling Basin	China	w	62	1.9	122	7
23	Dongfang	China	w	74	0.7	98	87
24	Sheep Mountain	Colorado	w	71	0.6	53	7
25	Sheep Mountain	Colorado	w	71	0.6	53	7
26	Pannonian System	Hungary	w	71	1.4	26	0
27	Pannonian System	Hungary	w	71	1.4	32	0
28	Velenje Basin	Slovenia	w	62	0.6	203	45
29	Colliery	Australia	w	72	0.7	241	268
30	Darkes Forest	Australia	w	65	1.2	786	1
31	Collinsville	Australia	w	65	1.2	788	15
32	Taranaki	New Zealand	w	68	1.3	36	0
33	Walbrzych coal basin	Poland	w	66	0.4	134	47
34	Chiayi-Yunshui	Taiwan	w	69	0.9	21	0
35	Platong	Thailand	w	63	0.6	305	256
36	Wildcat	West Virginia	w	51	2.4	1979	0
37	Indian creek	Wyoming	w	99	0.3	529	898
38	Labarge platform	Wyoming	w	139	3.7	125	0

Tab.3: Values of heat flux (mW/m^2), sediment thickness (km), distance from nearest volcano (km) and distance from nearest hydrocarbon field (km) for the recognized SHGS.

Geological factor	Samples	Mean	Conf. limit	Conf. limit	Median	Minimum	Maximum	Std.Dev.
a	38	114.4	**77.5**	**156.1**	72.5	51.0	453.0	111.5
b	38	1.8	**1.3**	**2.4**	1.3	0.1	5.9	1.6
c	38	188.1	**73.3**	**302.9**	69.4	3.5	1949.2	349.23
d	38	120.5	**57.5**	**183.5**	41.6	0.0	897.9	191.7

Tab.4: Confidence limit values relative to the selected geological factors: a) heat flux (mW/m^2); b) sediment thickness (km); c) distance from nearest volcano (km); d) distance from nearest hydrocarbon fields (km).

Sediment-Hosted Geothermal Systems: review and first global mapping

Procesi M.[1], Ciotoli G. [2,1], Mazzini A.[3], Etiope G.[1,4]

[1] Istituto Nazionale di Geofisica e Vulcanologia, Via di Vigna Murata 605, 00143 Roma, Italy
[2] Istituto di Geologia Ambientale e Geoingegneria—CNR-IGAG, Roma, Italy Centre for Earth
[3] Centre for Earth Evolution and Dynamics (CEED), University of Oslo, Norway
[4] Faculty of Environm. Science and Engineering, Babes Bolyai University, Cluj-Napoca, Romania

SUPPLEMENTARY MATERIAL

ID	SITE	COUNTRY	TYPE	CO_2 %	N_2 %	O_2 %	CH_4 %	H_2 %	H_2S %	He %	Ar %	$\delta^{13}C$ CO_2	$\delta^{13}C$ CH_4	$\delta^{2}H$ CH_4	R/Ra	Ref
1	Deception Island 1	Antarctica	G	98.4	0.820	0.145	0.002	0.068	0.513		0.018					[1]
2	Deception Island 2	Antarctica	G	98.3	0.837	0.203	0.003	0.012	0.591		0.018					[1]
3	Deception Island 3	Antarctica	G	98.6	0.571	0.050	0.005	0.150	0.604		0.012					[1]
4	Copahue volcano 7	Argentina	V	98.5	0.030	0.001	0.019	0.017	1.411		0.000					[1]
5	Copahue volcano 8	Argentina	V	96.0	0.380	0.023	0.068	1.647	1.774		0.002					[1]
6	Copahue volcano 5	Argentina	V	98.9	0.270	0.003	0.366	0.246	0.248		0.001					[1]
7	Copahue volcano 3	Argentina	V	98.0	0.694	0.007	0.369	0.429	0.539		0.002					[1]
8	Copahue volcano 6	Argentina	V	97.3	0.871	0.009	0.397	0.616	0.779		0.003					[1]
9	Copahue volcano 4	Argentina	V	97.0	0.668	0.019	0.576	0.555	1.139		0.003					[1]
10	Copahue volcano 1	Argentina	V	96.1	1.452	0.019	0.644	0.712	1.043		0.006					[1]
11	Copahue volcano 2	Argentina	V	95.8	1.456	0.012	0.648	1.042	0.990		0.005					[1]
12	Copahue volcano 9	Argentina	V	93.8	2.591	0.349	1.027	1.076	1.017		0.050					[1]
13	Copahue volcano 10	Argentina	V	93.5	1.277	0.023	2.696	0.503	2.005		0.006					[1]
14	LSTG-14	Chile	G	92.6	2.2	0.004	0.002	1.4	0.03	0.0003	0.002					[2]
15	LSTG-15	Chile	G	92.7	2.7	0.006	0.002	0.89	0.05	0.0002	0.003					[2]
16	LSTG-17	Chile	G	92.5	3.1	0.002	0.002	1.3	0.05	0.0002	0.002					[2]
17	Lascar volcano 9	Chile	V	85.6	6.716	0.065	0.002	1.215	0.151		0.008					[2]
18	LSTG-16	Chile	G	94.6	2.2	0.011	0.002	0.92	0.07	0.0004	0.004					[2]
19	LSTG-18	Chile	G	91.6	2.9	0.002	0.002	1.4	0.05	0.0002	0.002					[2]
20	LSTG-27	Chile	G	92.3	2.1	0.008	0.002	1.2	0.03	0.0002	0.003					[2]
21	Tacora volcano 4	Chile	V	95.1	1.346	0.004	0.002	0.009	2.760		0.001					[1]
22	Tacora volcano 6	Chile	V	94.2	1.454	0.001	0.002	0.012	3.619		0.002					[1, 2]
23	LSTG-26	Chile	G	93.7	1.7	0.003	0.003	0.98	0.06	0.0002	0.002					[2]
24	Tacora volcano 5	Chile	V	95.9	1.364	0.006	0.003	0.012	2.233		0.002					[1]
25	Lascar volcano 8	Chile	V	91.1	3.663	0.053	0.003	0.666	0.154		0.006					[1]
26	Tacora volcano 7	Chile	V	95.2	1.238	0.003	0.003	0.011	2.915		0.002					[1]
27	Tacora volcano 9	Chile	V	94.3	1.419	0.003	0.003	0.011	3.595		0.002					[1]
28	Tacora volcano 10	Chile	V	94.8	1.322	0.002	0.004	0.010	3.322		0.001					[1]
29	LSTG-23	Chile	G	96.6	0.32	0.000	0.004	0.02	1.1	0.0003	0.001					[2]
30	LSTG-13	Chile	G	95.1	2.0	0.002	0.004	0.93	0.39	0.0001	0.003					[2]
31	LSTG-25	Chile	G	95.5	0.34	0.001	0.004	0.03	1.7	0.0004	0.001					[2]
32	LSTG-4	Chile	G	95.2	0.65	0.002	0.004	0.02	2.5	0.0002	0.001					[2]
33	LSTG-22	Chile	G	95.9	0.36	0.000	0.004	0.02	1.1	0.0004	0.000					[2]
34	LSTG-28	Chile	G	94.9	2.1	0.004	0.004	0.80	0.11	0.0001	0.002					[2]
35	Tacora volcano 8	Chile	V	94.8	1.355	0.003	0.004	0.013	3.107		0.002					[1]
36	Lascar volcano 12	Chile	V	85.4	7.467	0.049	0.004	0.859	0.184		0.013					[1]
37	Lascar volcano 10	Chile	V	84.1	9.258	0.068	0.005	0.629	0.182		0.009					[1]
38	LSTG-20	Chile	G	94.2	0.38	0.001	0.005	0.03	3.2	0.0005	0.001					[2]
39	LSTG-6	Chile	G	94.9	0.53	0.002	0.005	0.03	2.7	0.0001	0.001					[2]
40	LSTG-21	Chile	G	95.2	0.39	0.001	0.005	0.03	1.8	0.0007	0.001					[2]
41	LSTG-24	Chile	G	95.7	0.39	0.000	0.005	0.03	1.5	0.0006	0.001					[2]

ID	SITE	COUNTRY	TYPE	CO_2 %	N_2 %	O_2 %	CH_4 %	H_2 %	H_2S %	He %	Ar %	$\delta^{13}C$ CO_2	$\delta^{13}C$ CH_4	$\delta^{2}H$ CH_4	R/Ra	Ref
42	LSTG-2	Chile	G	94.0	2.8	0.041	0.005	0.70	0.03	0.0002	0.002					[2]
43	Lascar volcano 11	Chile	V	84.0	8.413	0.051	0.005	0.892	0.199		0.013					[1]
44	LSTG-3	Chile	G	93.9	2.7	0.036	0.005	0.71	0.03	0.0002	0.002					[2]
45	LSTG-5	Chile	G	95.2	0.81	0.005	0.005	0.00	2.2	0.0002	0.001					[2]
46	Lascar volcano 7	Chile	V	83.5	8.111	0.062	0.005	1.612	0.198		0.009					[1]
47	LSTG-11	Chile	G	93.1	2.8	0.009	0.006	1.1	0.05	0.0002	0.002					[2]
48	LSTG-1	Chile	G	92.9	3.0	0.050	0.006	0.91	0.04	0.0002	0.003					[2]
49	LSTG-12	Chile	G	94.7	1.9	0.016	0.006	1.1	0.39	0.0002	0.003					[2]
50	LSTG-10	Chile	G	92.0	3.5	0.009	0.006	1.1	0.11	0.0002	0.002					[2]
51	LSTG-9	Chile	G	99.0	0.45	0.000	0.007	0.01	0.42	0.0005	0.001					[2]
52	LSTG-8	Chile	G	98.9	0.47	0.000	0.007	0.01	0.43	0.0006	0.001					[2]
53	LSTG-29	Chile	G	98.5	0.74	0.001	0.007	0.05	0.49	0.0007	0.002					[2]
54	El Tatio 2	Chile	G	99.0	0.628	0.003	0.008	0.020	0.367		0.005					[1]
55	LSTG-7	Chile	G	98.9	0.51	0.000	0.008	0.01	0.45	0.0010	0.001					[2]
56	LSTG-19	Chile	G	98.7	0.67	0.001	0.009	0.04	3.46	0.0008	0.002					[2]
57	LSTG-30	Chile	G	98.6	0.60	0.001	0.009	0.04	0.44	0.0009	0.003					[2]
58	El Tatio 1	Chile	G	99.0	0.655	0.003	0.012	0.011	0.329		0.004					[1]
59	El Tatio 3	Chile	G	99.3	0.448	0.006	0.020	0.014	0.202		0.004					[1]
60	El Tatio 4	Chile	G	99.3	0.580	0.006	0.022	0.016	0.118		0.006					[1]
61	Tacora volcano 1	Chile	V	85.3	11.184	0.001	0.022	0.087	2.680		0.012					[1]
62	Lascar volcano 6	Chile	V	76.6	16.744	0.077	0.023	2.055	0.818		0.026					[1]
63	Lascar volcano 5	Chile	V	76.8	14.400	0.029	0.027	2.068	0.860		0.033					[1]
64	Tacora volcano 2	Chile	V	87.4	9.496	0.014	0.027	0.086	2.518		0.008					[1]
65	Tacora volcano 3	Chile	V	80.6	15.648	0.081	0.029	0.154	2.886		0.016					[1]
66	El Tatio 5	Chile	G	99.3	0.547	0.005	0.042	0.009	0.073		0.005					[1]
67	Lascar volcano 4	Chile	V	74.4	18.630	0.060	0.043	2.024	1.030		0.098					[1]
68	Lascar volcano 1	Chile	V	75.4	20.721	0.046	0.049	1.927	0.444		0.129					[1]
69	Lascar volcano 3	Chile	V	75.5	20.099	0.056	0.069	1.823	0.526		0.142					[1]
70	Lascar volcano 2	Chile	V	78.5	17.906	0.046	0.073	1.592	0.480		0.123					[1]
71	PGM21	Costa Rica	G	99.1	0.770		0.029	0.080					-29.9		6.81	[3]
72	PGM11	Costa Rica	G	99.6	0.380		0.016	0.040					-27.4		6.86	[3]
73	PGM05	Costa Rica	G	99.0	0.890		0.025	0.030					-24.1		6.23	[3]
74	PGM29	Costa Rica	G	99.8	0.007		0.180	0.000					-22.8		6.68	[3]
75	PGM45	Costa Rica	G	95.1	0.107		4.370	0.170					-16.6		6.66	[3]
76	Rincon de la Vieja	Costa Rica	V	97.8	0.300	0.038	0.000	0.021	1.400	0.000	0.002					[4]
77	Turrialba volcano 1	Costa Rica	V	91.5	0.942	0.000	0.000	0.030	6.904		0.001					[1]
78	Turrialba volcano 3	Costa Rica	V	96.6	0.054	0.000	0.000	0.116	1.725		0.000					[1]
79	Turrialba volcano 4	Costa Rica	V	96.4	0.551	0.001	0.000	0.363	2.007		0.001					[1]
80	Turrialba volcano 2	Costa Rica	V	90.8	1.423	0.006	0.000	0.005	7.364		0.002					[1]
81	CAS02	Costa Rica	G	99.4	0.550		0.002	0.010							4.34	[3]
82	PGM01	Costa Rica	G	98.2	1.370		0.025	0.320							6.52	[3]
83	PGM10	Costa Rica	G	98.7	1.070		0.028	0.120							6.64	[3]
84	PGM03	Costa Rica	G	97.8	1.930		0.035	0.090								[3]
85	PGM12	Costa Rica	G	98.4	1.190		0.040	0.310							6.49	[3]
86	PGM03	Costa Rica	G	96.2	3.450		0.042	0.200								[3]
87	PGM20	Costa Rica	G	93.3	6.290		0.144	0.070							6.67	[3]
88	PGM02	Costa Rica	G	96.4	3.100		0.150	0.260							7.15	[3]
89	PGM31	Costa Rica	G	98.8	0.019		1.010	0.080							6.24	[3]
90	VPOCL	Costa Rica	G	97.4	0.027		1.830	0.050							7.15	[3]
91	PGM46	Costa Rica	G	97.1	0.052		2.530	0.060							6.55	[3]
92	AH23	El Salvador	G	98.4	1.470		0.013	0.090							7.07	[3]
93	AH17	El Salvador	G	97.9	1.740		0.015	0.210							7	[3]
94	SV01	El Salvador	G	95.7	3.450		0.019	0.540							6.34	[3]
95	TR09	El Salvador	G	72.1	23.190		0.020	0.200							5.71	[3]
96	LV01	El Salvador	G	51.8	31.690		0.020	0.370							3.47	[3]
97	IF01	El Salvador	G	83.6	11.040		0.020	0.270							5.95	[3]
98	TR4B	El Salvador	G	96.1	3.480		0.027	0.310							5.8	[3]
99	TR02	El Salvador	G	95.3	4.200		0.030	0.230							5.59	[3]
100	AH22	El Salvador	G	96.7	3.000		0.036	0.200							6.86	[3]
101	AH20	El Salvador	G	96.8	2.580		0.038	0.380							6.93	[3]
102	AH06	El Salvador	G	93.4	5.980		0.049	0.340							7.01	[3]

ID	SITE	COUNTRY	TYPE	CO_2 %	N_2 %	O_2 %	CH_4 %	H_2 %	H_2S %	He %	Ar %	$\delta^{13}C$ CO_2	$\delta^{13}C$ CH_4	$\delta^{2}H$ CH_4	R/Ra	Ref
103	AH4B	El Salvador	G	97.2	2.510		0.056	0.220							6.9	[3]
104	SV02	El Salvador	G	95.9	3.300		0.068	0.520							6.48	[3]
105	AH21	El Salvador	G	96.8	2.550		0.070	0.350							7.08	[3]
106	TR4C	El Salvador	G	93.1	6.470		0.093	0.210							5.54	[3]
107	AH16A	El Salvador	G	87.9	10.970		0.244	0.200							6.77	[3]
108	EPR	EPR	V									-7	-15	-102		[5]
109	Afar 6	Ethiopia	V	96.5	1.574	0.520	0.060	0.003	1.254		0.038					[1]
110	Afar 7	Ethiopia	V	97.5	0.904	0.288	0.090	0.001	1.171		0.022					[1]
111	Afar 2	Ethiopia	V	97.4	0.809	0.348	0.115	0.242	1.082		0.019					[1]
112	Afar 4	Ethiopia	V	96.0	2.049	0.572	0.116	0.001	1.248		0.051					[1]
113	Afar 1	Ethiopia	V	97.2	1.823	0.393	0.121	0.001	0.362		0.044					[1]
114	Afar 3	Ethiopia	V	97.4	0.753	0.230	0.141	0.239	1.228		0.018					[1]
115	Afar 5	Ethiopia	V	97.1	0.722	0.248	0.203	0.268	1.437		0.016					[1]
116	Milos	Greece	G	61.6			1.300					0.4	-17.8	-149		[6]
117	Milos	Greece	G	56.3			0.514					0.7	-14.7	-146		[6]
118	Milos	Greece	G	70.1			0.929					1.1	-13.7	-189		[6]
119	Milos	Greece	G	67.8			0.300					-0.2	-11.6	-166		[6]
120	Milos	Greece	G	61.4			0.488					0	-10.1	-126		[6]
121	Milos	Greece	G	74.3			0.463					0.3	-9.4	-132		[6]
122	Nysiros Island 14	Greece	G	82.7	0.023	0.000	0.012	0.225	17.032		0.000					[1]
123	Nysiros Island 9	Greece	G	82.2	0.072	0.001	0.020	0.112	17.613		0.000					[1]
124	Nysiros Island 2	Greece	G	86.7	0.017	0.000	0.038	0.099	13.103		0.000					[1]
125	Nysiros Island 6	Greece	G	82.5	0.406	0.004	0.055	1.896	15.118		0.002					[1]
126	Nysiros Island 10	Greece	G	77.9	0.058	0.000	0.185	0.802	21.084		0.000					[1]
127	Nysiros Island 4	Greece	G	82.1	0.078	0.001	0.217	0.320	17.320		0.000					[1]
128	Nysiros Island 5	Greece	G	82.8	0.058	0.000	0.230	0.360	16.594		0.000					[1]
129	Nysiros Island 13	Greece	G	82.3	1.034	0.000	0.275	0.341	16.068		0.004					[1]
130	Nysiros Island 3	Greece	G	84.7	0.193	0.001	0.756	0.677	13.645		0.001					[1]
131	Nysiros Island 11	Greece	G	82.1	1.016	0.029	1.051	1.402	14.385		0.003					[1]
132	Nysiros Island 1	Greece	G	77.3	0.258	0.001	1.190	1.065	20.137		0.001					[1]
133	Nysiros Island 12	Greece	G	89.5	1.131	0.020	2.295	0.971	6.077		0.003					[1]
134	Nysiros Island 8	Greece	G	78.2	0.279	0.002	2.568	2.745	16.234		0.001					[1]
135	Nysiros Island 7	Greece	G	73.3	1.304	0.009	3.119	5.334	16.955		0.004					[1]
136	G0703	Iceland	G	97.4	2.30		0.015		0.06							[7]
137	G0713	Iceland	G	96.8	0.69		0.015		2.16							[7]
138	G0715	Iceland	G	94.0	0.75		0.017		3.65							[7]
139	Reykjanes	Iceland	G	93.3	1.790		0.018	1.104	3.799		0.026					[7]
140	G0701	Iceland	G	91.6	1.63		0.019		4.96							[7]
141	G0704	Iceland	G	92.0	2.04		0.019		4.69							[7]
142	G0711	Iceland	G	91.4	1.50		0.019		5.78							[7]
143	G0712	Iceland	G	91.3	1.63		0.019		5.58							[7]
144	G0716	Iceland	G	96.6	0.66		0.019		1.93							[7]
145	G0709	Iceland	G	90.0	5.09		0.020		3.82							[7]
146	G0707	Iceland	G	91.6	1.64		0.021		5.36							[7]
147	The Hole	Italy	G	79.9	19.300	0.130	0.590	0.001			0.100	3.7		-176		[8]
148	Bagni di Tivoli	Italy	G	98.1	1.700	0.001	0.033	0.000	0.130		0.026	-5.2	-36.4	-161		[8]
149	Vesuvio	Italy	V	99.5	0.390	0.018	0.059	0.000	0.010		0.009	-6.7	-36.1	-138		[8]
150	Fosso S.Antonino	Italy	G	96.1	3.300	0.062	0.190	0.002	0.210	0.000	0.075	1.02	-33.4	-166	1.04	[9]
151	Bullicame	Italy	G	98.0	1.000	0.005	0.014	0.000	1.000		0.004	-1.3	-31.3	-158		[8]
152	acqua forte ponzano	Italy	G	96.6	3.200	0.039	0.085	0.000	0.029	0.000	0.076	-0.47	-31.2	-165	0.88	[9]
153	monte caio	Italy	G	96.8	2.900	0.240	0.016	0.001	0.033	0.000	0.055	-4.73	-30.6	-154	0.74	[9]
154	Bagni di Tivoli	Italy	G	96.8	2.800	0.220	0.033	0.000	0.140		0.035	0.9	-30.1	-135		[8]
155	Bagni di S.Filippo	Italy	G	98.7	1.100	0.170	0.016	0.000	0.010		0.019	-1.1	-29.4	-135		[8]
156	Solfatara Pomezia	Italy	G	99.2	0.680	0.022	0.004	0.000	0.068		0.013	-2.1	-29.3	-139		[8]
157	Trevignano	Italy	G	96.6	3.100	0.091	0.037	0.002	0.110	0.000	0.062	0.26	-29.2	-155	0.61	[9]
158	Lago Vico	Italy	G	99.0	0.700	0.006	0.270	0.002		0.000		-3.1	-28.9	-176	0.77	[10]
159	Acqua Forte	Italy	G	99.2	0.790	0.010	0.006	0.001	0.008	0.000	0.013	-1.9	-28.4	-168	0.69	[10]
160	Le Zitelle	Italy	G	99.4	0.570	0.017	0.024	0.006	0.009	0.001	0.010	-2.3	-28.1	-156	1.19	[10]
161	Lagoni Rossi	Italy	G	92.6	5.200	0.001	2.100	0.000	0.002		0.007	-1.1	-28.1	-164		[8]
162	Latera1	Italy	G	97.7	1.600	0.080	0.255	0.000	0.400		0.010	0.2	-27.9	-139		[8]
163	San Filippo	Italy	G	95.3	2.003	0.002	1.713		0.142	0.001	0.001	-3.33	-27.8	-143		[11]

ID	SITE	COUNTRY	TYPE	CO_2 %	N_2 %	O_2 %	CH_4 %	H_2 %	H_2S %	He %	Ar %	$\delta^{13}C$ CO_2	$\delta^{13}C$ CH_4	$\delta^{2}H$ CH_4	R/Ra	Ref
164	Torre Alfina	Italy	G	99.0	0.840	0.000	0.120	0.000	0.042		0.003	0.4	-27.3	-131		[8]
165	Bagnaccio	Italy	G	99.3	0.660	0.011	0.037	0.006	0.014	0.000	0.010	-2	-26.9	-150	0.65	[10]
166	S. Cristoforo	Italy	G	99.1	0.810	0.017	0.061	0.004	0.010	0.000	0.014	-2.4	-26.7	-153	0.9	[10]
167	Le Zitelle	Italy	G	99.1	0.790	0.007	0.062	0.003	0.023	0.000	0.013	1.1	-26.6	-148	0.67	[10]
168	Masse S.Sisto	Italy	G	99.2	0.760	0.016	0.035	0.005	0.011	0.000	0.012	-2.6	-26.4	-155	0.69	[10]
169	Sasso Pisano	Italy	G	92.3	0.580	0.000	2.400	2.800	1.800		0.009	-3.2	-26.4	-136		[8]
170	Solfatara di Nepi	Italy	G	99.4	0.540	0.006	0.007	0.002	0.043	0.000	0.005	-1.2	-26.3	-149	0.55	[10]
171	Foralupo	Italy	G	99.3	0.610	0.012	0.068	0.006	0.014	0.000	0.008	0.23	-26.3	-153	0.56	[10]
172	Muralto (o Montecchie)	Italy	G	99.1	0.750	0.017	0.070	0.002	0.016	0.000	0.009	-0.73	-26.1	-166	0.57	[10]
173	Lo Spuntone	Italy	G	89.0	4.500	0.720	1.000	3.700	1.000		0.045	-3.7	-25.9	-161		[8]
174	Caldara Manziana	Italy	G	99.1	0.664	0.001	0.217	0.000	0.054	0.000	0.001	-2.79	-25.7	-101	0.59	[12]
175	Zancona	Italy	G	95.5	0.320	0.010	4.100				0.008	-1.8	-25.6	-144		[8]
176	Grotte S.Stefano	Italy	G	99.4	0.500	0.005	0.023	0.007	0.021	0.000	0.007	0.28	-25.5	-145	0.5	[10]
177	Bullicame	Italy	G	99.3	0.600	0.010	0.016	0.005	0.022	0.000	0.012	-1.2	-25.3	-144	0.69	[10]
178	castel campanile	Italy	G	96.0	3.600	0.021	0.270	0.002		0.000	0.071	-1.69	-25.2	-160	0.07	[9]
179	Mola di Bassano	Italy	G	99.3	0.600	0.010	0.035	0.004	0.002	0.000	0.006	-1.1	-25.1	-147		[10]
180	Tor Caldara	Italy	G	99.7	0.320	0.006	0.022	0.000			0.008	-0.9	-24.8	-143		[8]
181	Foralupo	Italy	G	98.8	0.690	0.004	0.390	0.002	0.099	0.000	0.008	0.49	-24.8	-151	0.46	[10]
182	Poggio dell'Ulivo	Italy	G	98.7	0.700	0.011	0.460	0.003	0.084	0.000	0.006	0.35	-24.8	-156	0.5	[10]
183	Sasso Pisano	Italy	G	90.7	0.717	0.033	2.152	2.238	3.226	0.001	0.003	-3.83	-23.7	-134		[13]
184	Monte Solferata	Italy	G	98.5	0.679	0.033	0.520	0.000	0.218	0.000	0.001	-1.14	-23.3	-132	0.37	[10]
185	Tuscania	Italy	G	99.1	0.840	0.022	0.008	0.002	0.033	0.000	0.013	-0.76	-22.6	-138	0.36	[10]
186	Favara Grande	Italy	G	91.4	0.700	0.005	2.500	3.000	2.400		0.006	-2.5	-22.3	-134		[8]
187	Parco di Diosilla	Italy	G	99.1	0.544	0.001	0.304	0.000	0.051	0.000	0.000	-1.83	-22.1	-152	0.57	[12]
188	Piana di Stigliano	Italy	G	99.2	0.382	0.003	0.402	0.000	0.057	0.000	0.001	-1.66	-21.2	-116	0.48	[12]
189	Pan1	Italy	G	99.1	0.160	0.022	0.001	0.030	0.660		0.003	-0.9	-20.6	-103		[8]
190	Parco della Mola	Italy	G	98.5	0.566	0.039	0.842	0.000	0.057	0.000	0.001	0	-20.4	-137	0.62	[12]
191	S.Pompeo	Italy	G	96.9	0.900	0.061	0.890	0.230	1.000		0.015	-1.1	-20.1	-106		[8]
192	Pan2	Italy	G	98.3	0.610	0.089	0.001	0.016	1.000		0.012	-1.5	-19.7	-111		[8]
193	Vejano	Italy	G	99.2	0.361	0.002	0.373	0.000	0.054	0.000	0.000	0.46	-19.5	-137	0.59	[12]
194	Pan3	Italy	G	98.5	0.400	0.031	0.001	0.031	1.000		0.008	-1.3	-19.3	-104		[8]
195	Solfatara (BG)	Italy	G	98.5	0.290	0.000	0.010	0.240	0.650		0.001	-0.9	-17.8			[8]
196	Favara Grande	Italy	G	97.7	0.194	0.006	0.736	0.835	0.481		0.003	-3.7	-17.6	-121		[14]
197	Ermeta	Italy	G	86.9	4.100	0.900	2.900	5.000	0.070		0.001	-3.7	-17.6	-121		[8]
198	Vulcano Island crater 17	Italy	V	96.9	1.934	0.012	0.000	0.015	0.863		0.002					[1]
199	Vulcano Island crater 7	Italy	V	95.3	1.684	0.075	0.000	0.231	0.540		0.006					[1]
200	Vulcano Island crater 11	Italy	V	95.0	1.131	0.003	0.000	0.095	1.679		0.001					[1]
201	Vulcano Island crater 16	Italy	V	98.2	0.906	0.003	0.000	0.108	0.640		0.001					[1]
202	Vulcano Island crater 5	Italy	V	96.8	1.111	0.000	0.000	0.064	0.458		0.001					[1]
203	Vulcano Island crater 2	Italy	V	93.3	1.626	0.104	0.000	0.190	0.853		0.002					[1]
204	Vulcano Island crater 6	Italy	V	99.3	0.308	0.000	0.000	0.009	0.358		0.000					[1]
205	Vulcano Island crater 4	Italy	V	95.1	0.853	0.001	0.000	0.887	2.512		0.002					[1]
206	Vulcano Island crater 13	Italy	V	92.0	1.290	0.001	0.000	0.156	3.116		0.002					[1]
207	Vulcano Island crater 3	Italy	V	88.1	2.687	0.151	0.000	0.095	1.529		0.004					[1]
208	Vulcano Island crater 9	Italy	V	96.8	1.090	0.000	0.000	0.055	1.056		0.001					[1]
209	Vulcano Island crater 18	Italy	V	95.2	0.741	0.003	0.000	1.819	2.064		0.002					[1]
210	Vulcano Island crater 10	Italy	V	91.6	4.004	0.014	0.000	1.130	2.098		0.004					[1]
211	Vulcano Island crater 1	Italy	V	93.0	2.735	0.168	0.000	0.034	0.831		0.004					[1]
212	Vulcano Island crater 14	Italy	V	95.1	1.705	0.138	0.000	0.730	0.448		0.002					[1]
213	Vulcano Island crater 8	Italy	V	93.3	4.460	0.023	0.000	0.041	2.092		0.014					[1]
214	VO2	Italy	V	48.5	48.900	0.878	0.000	0.385	0.062	0.001	0.560					[8]
215	SE2	Italy	V	52.2	43.200	3.660	0.000	0.134	0.026	0.001	0.440					[8]
216	VO1	Italy	V	50.7	46.700	0.665	0.000	0.417	0.056	0.001	0.520					[8]
217	BN1	Italy	V	69.7	26.600	2.860	0.000	0.156	0.029	0.001	0.250					[8]
218	Vulcano Island crater 12	Italy	V	92.7	1.732	0.000	0.000	0.446	1.380		0.001					[1]
219	BN2	Italy	V	68.0	28.400	2.660	0.000	0.274	0.025	0.000	0.240					[8]
220	Vulcano Island crater 19	Italy	V	84.8	2.594	0.256	0.000	3.259	3.615		0.003					[1]
221	Pantelleria Island 2	Italy	G	97.8	1.427	0.395	0.001	0.000	0.305		0.037					[1]
222	Vulcano Island crater 15	Italy	V	92.1	2.021	0.010	0.001	0.848	2.303		0.004					[1]
223	SE1	Italy	V	53.4	41.100	4.750	0.001	0.081	0.015	0.000	0.450					[8]
224	VOF7	Italy	V	95.5	2.000	0.056	0.001	0.001	0.845	0.002	0.018					[8]

ID	SITE	COUNTRY	TYPE	CO_2 %	N_2 %	O_2 %	CH_4 %	H_2 %	H_2S %	He %	Ar %	$\delta^{13}C$ CO_2	$\delta^{13}C$ CH_4	$\delta^{2}H$ CH_4	R/Ra	Ref
225	SE3	Italy	V	54.3	38.700	6.290	0.001	0.111	0.032	0.000	0.410					[8]
226	Ischia Island 5	Italy	V	91.9	5.829	1.832	0.002	0.021	0.396		0.025					[1]
227	Ischia Island 1	Italy	V	91.3	6.675	1.707	0.002	0.017	0.226		0.026					[1]
228	Ischia Island 2	Italy	V	96.0	2.603	1.076	0.002	0.020	0.243		0.010					[1]
229	Phlegrean Fields 10	Italy	V	99.0	0.141	0.001	0.003	0.086	0.803		0.000					[1]
230	Phlegrean Fields 6	Italy	V	98.6	0.200	0.002	0.003	0.130	1.097		0.000					[1]
231	Phlegrean Fields 1	Italy	V	99.5	0.116	0.003	0.003	0.067	0.273		0.001					[1]
232	Phlegrean Fields 7	Italy	V	98.7	0.184	0.001	0.004	0.134	0.986		0.000					[1]
233	Phlegrean Fields 4	Italy	V	98.7	0.180	0.007	0.004	0.134	0.891		0.001					[1]
234	Phlegrean Fields 3	Italy	V	98.9	0.182	0.001	0.005	0.106	0.824		0.001					[1]
235	Ischia Island 4	Italy	V	98.1	0.556	0.027	0.005	0.746	0.517		0.003					[1]
236	Phlegrean Fields 8	Italy	V	98.4	0.240	0.003	0.005	0.210	1.087		0.000					[1]
237	Phlegrean Fields 9	Italy	V	97.7	0.269	0.001	0.005	0.219	1.742		0.000					[1]
238	Phlegrean Fields 2	Italy	V	99.4	0.172	0.001	0.006	0.100	0.309		0.001					[1]
239	Ischia Island 3	Italy	V	98.7	0.915	0.068	0.012	0.055	0.272		0.003					[1]
240	Phlegrean Fields 5	Italy	V	97.3	0.793	0.002	0.015	0.778	1.109		0.003					[1]
241	Pantelleria Island 1	Italy	G	99.5	0.143	0.004	0.019	0.000	0.314		0.004					[1]
242	Phlegrean Fields 11	Italy	V	98.2	0.221	0.002	0.020	0.146	1.381		0.000					[1]
243	TF	Italy	V	39.4	52.500	7.520	0.029	<0.0001	<0.001	0.001	0.580					[8]
244	Vesuvio volcano 2	Italy	V	97.5	0.196	0.002	0.041	0.753	1.455		0.001					[1]
245	Vesuvio volcano 1	Italy	V	97.3	0.400	0.003	0.042	0.762	1.422		0.001					[1]
246	Larderello 4	Italy	G	83.4	10.238	2.764	0.406	2.116	0.898		0.147					[1]
247	Larderello 2	Italy	G	73.6	19.500	4.615	0.425	0.907	0.676		0.273					[1]
248	Pantelleria Island 3	Italy	G	97.7	0.194	0.006	0.736	0.835	0.481		0.003					[1]
249	Larderello 3	Italy	G	93.6	1.389	0.028	0.902	2.769	1.303		0.006					[1]
250	BT	Italy	V	61.7	35.600	1.190	1.200	0.021	<0.001	0.001	0.310					[8]
251	Larderello 1	Italy	G	92.5	1.505	0.028	1.446	2.036	2.513		0.005					[1]
252	Larderello 5	Italy	G	91.4	1.574	0.015	2.442	2.788	1.827		0.009					[1]
253	Issaikyo	Japan	V	86.6	5.780		0.006	0.061	7.330		0.023					[15]
254	Galion	L. Antilles	G	72.1	8.000	0.000	0.000	0.856	18.600	0.003	0.044					[16]
255	Penville	L. Antilles	G	74.6	6.000	0.625	0.000	0.000	17.700	0.020	0.717					[16]
256	Sulphur springs	L. Antilles	G	77.7	8.600	2.389	0.000	0.004	10.900	0.000	0.000					[16]
257	Sulphur Springs	L. Antilles	G	98.6	0.600	0.000	0.001	0.235	0.900	0.001	0.007					[16]
258	Galion	L. Antilles	G	67.2	12.100	0.857	0.002	1.152	17.400	0.011	0.741					[16]
259	Galion	L. Antilles	G	93.7	5.500	0.370	0.002	0.467	0.700	0.003	0.003					[16]
260	Sulphur springs	L. Antilles	G	76.9	5.800	0.000	0.005	0.563	16.100	0.002	0.000					[16]
261	Valley of Desolation	L. Antilles	G	80.0	2.200	0.108	0.008	0.333	16.500	0.000	595.000					[16]
262	Valley of Desolation	L. Antilles	G	71.9	11.600	1.058	0.012	0.441	14.100	0.000	0.000					[16]
263	Sulphur Springs	L. Antilles	G	97.7	0.800	0.000	0.013	1.475	0.700	0.000	0.003					[16]
264	Valley of Desolation	L. Antilles	G	96.5	1.100	0.001	0.014	0.000	2.400	0.474	0.004					[16]
265	Watten Waven	L. Antilles	G	99.3	0.500	0.001	0.014	0.152	1.300	0.002	0.006					[16]
266	Valley of Desolation	L. Antilles	G	96.5	0.400	0.002	0.015	0.750	10.800	0.000	0.004					[16]
267	Valley of Desolation	L. Antilles	G	50.2	9.000	0.000	0.030	5.494	32.900	0.000	0.158					[16]
268	Watten Waven	L. Antilles	G	98.3	1.300	0.001	0.034	0.305	0.500	0.000	0.009					[16]
269	Valley of Desolation	L. Antilles	G	97.6	2.200	0.000	0.066	0.000	1.500	0.913	0.012					[16]
270	Watten Waven	L. Antilles	G	78.4	2.000	0.000	0.070	0.618	18.600	0.005	0.018					[16]
271	Valley of Desolation	L. Antilles	G	67.0	6.330	0.380	0.078	2.980	22.000		0.031					[16]
272	Watten Waven	L. Antilles	G	68.9	10.500	2.035	0.088	0.791	15.700	0.007	1.690					[16]
273	Valley of Desolation	L. Antilles	G	71.4	2.500	0.000	0.116	4.541	19.900	0.000	0.012					[16]
274	Champagne	L. Antilles	G	93.4	5.900	0.024	0.161	0.001	0.200	0.029	0.165					[16]
275	Champagne	L. Antilles	G	76.2	4.700	0.381	0.178	0.000	2.800	0.008	0.289					[16]
276	Valley of Desolation	L. Antilles	G	49.2	5.200	0.000	0.216	8.163	35.400	0.000	0.032					[16]
277	Penville	L. Antilles	G	73.1	3.500	0.000	0.661	0.001	18.100	0.007	0.005					[16]
278	El Chichon volcano 6	Mexico	V	92.5	2.051	0.021	0.003	1.945	3.442		0.010					[1]
279	El Chichon volcano 3	Mexico	V	95.3	1.398	0.050	0.004	1.046	2.235		0.007					[1]
280	El Chichon volcano 1	Mexico	V	93.5	1.264	0.039	0.005	3.447	1.787		0.008					[1]
281	El Chichon volcano 2	Mexico	V	97.4	0.339	0.000	0.008	0.788	1.509		0.001					[1]
282	El Chichon volcano 5	Mexico	V	82.6	10.124	0.259	0.010	5.443	1.492		0.035					[1]
283	El Chichon volcano 4	Mexico	V	91.3	1.510	0.017	0.023	1.295	5.873		0.004					[1]
284	Women Bath	New Mexico	G	98.5	0.690	0.004	0.016	0.100				-3.6			6.16	[17]
285	Men Bath	New Mexico	G	98.3	0.890	0.033	0.021	0.170				-4.63				[17]

ID	SITE	COUNTRY	TYPE	CO_2 %	N_2 %	O_2 %	CH_4 %	H_2 %	H_2S %	He %	Ar %	$\delta^{13}C$ CO_2	$\delta^{13}C$ CH_4	$\delta^{2}H$ CH_4	R/Ra	Ref
286	Tony	New Mexico	G	98.8	0.420	0.007	0.022	0.290								[17]
287	Main Fumarole	New Mexico	G	99.0	0.250	0.002	0.033	0.044								[17]
288	Footbath Spring	New Mexico	G	97.9	0.620	0.030	0.064	0.480				-2.47			5.16	[17]
289	Waikite	New Zealand	G	87.0	12.000		1.000									[18]
290	Ngatamariki	New Zealand	G	93.0	1.500		2.400			0.001						[18]
291	Ngawha	New Zealand	G	93.1	0.600		4.200									[18]
292	MT40	Nicaragua	G	93.2	6.080		0.325	0.110					-24.6		6.99	[3]
293	MT27	Nicaragua	G	95.1	4.030		0.288	0.240					-24.2		6.75	[3]
294	MT36-43	Nicaragua	G	94.2	4.170		1.182	0.460					-23.9		6.96	[3]
295	MT43	Nicaragua	G	93.9	3.980		1.343	0.780					-23.5		6.72	[3]
296	4	Nicaragua	G	98.6	0.720		0.007	0.680							7.37	[3]
297	1026	Nicaragua	G	92.9	6.960		0.010	0.000							7.69	[3]
298	1025	Nicaragua	G	91.1	5.900		0.091	0.510							7.04	[3]
299	1023	Nicaragua	G	92.7	5.760		0.148	0.380							6.79	[3]
300	1024	Nicaragua	G	93.0	4.960		0.183	0.460							6.79	[3]
301	3	Nicaragua	G	80.1	0.370		0.183	19.310							7.72	[3]
302	MT38	Nicaragua	G	94.8	4.690		0.242	0.140							6.74	[3]
303	MT35	Nicaragua	G	95.5	4.080		0.260	0.110							6.76	[3]
304	2	Nicaragua	G	85.3	14.180		0.267	0.050							7.5	[3]
305	MT20	Nicaragua	G	95.4	4.110		0.305	0.150							6.71	[3]
306	MT38A	Nicaragua	G	90.0	8.570		0.421	0.090							7.05	[3]
307	MT35	Nicaragua	G	95.1	4.280		0.424	0.100							6.75	[3]
308	MT42	Nicaragua	G	95.4	3.900		0.436	0.200							6.79	[3]
309	MT40B	Nicaragua	G	93.9	5.540		0.442	0.070							7.04	[3]
310	MT42	Nicaragua	G	94.3	4.950		0.458	0.180							6.78	[3]
311	MT27	Nicaragua	G	91.3	7.930		0.484	0.110							6.8	[3]
312	Cagua	Philippines	G	93.0	1.350	<0.004	0.000	1.250								[19]
313	MAMt Apo	Philippines	G	95.7	2.300	0.004	0.003	0.391								[19]
314	DA	Philippines	G	84.6	0.580		0.056	2.070	12.400							[20]
315	DC	Philippines	G	84.0	0.340		0.078	2.810	12.800							[20]
316	DB	Philippines	G	87.6	0.610		0.085	2.760	8.900							[20]
317	DJ	Philippines	G	89.4	0.760	0.181	0.218	1.200	8.200							[20]
318	BD	Philippines	G	98.4	0.110	0.113	0.251	0.000	0.100		0.013					[20]
319	DE	Philippines	G	92.7	0.190		0.340	4.310	2.400							[20]
320	BA	Philippines	G	97.1	0.290		0.367	0.020	1.800							[20]
321	DF	Philippines	G	92.2	0.250		0.428	5.080	2.200							[20]
322	BB	Philippines	G	97.7	0.800		0.451	0.001	1.000							[20]
323	DW	Philippines	G	94.6	0.480	<0.004	0.530	2.390	2.100	0.000	0.003					[20]
324	DG	Philippines	G	94.4	0.430	0.015	0.586	2.110	2.500		0.005					[20]
325	DH	Philippines	G	94.3	0.260	0.003	0.621	2.070	2.700		0.003					[20]
326	BC	Philippines	G	93.9	0.123		0.701	0.004	1.100							[20]
327	DD	Philippines	G	92.4	0.640	0.210	0.908	4.200	1.700							[20]
328	DI	Philippines	G	87.7	0.940	0.158	1.225	2.300	7.700							[20]
329	Mambucal	Philippines	G	95.5	2.970	<0.004	1.290	0.042								[19]
330	Mambucal	Philippines	G	95.5	2.970		1.290	0.039		0.002	0.004					[19]
331	Teide volcano 1	Spain	V	96.0	1.544	0.069	0.002	0.419	1.781		0.022					[1]
332	Teide volcano 2	Spain	V	96.9	0.770	0.042	0.002	0.504	1.684		0.008					[1]
333	Tatun 6	Taiwan	G	95.0	4.845	0.030	0.047	0.001	0.083		0.011					[1]
334	Tatun 4	Taiwan	G	97.6	2.074	0.015	0.053	0.001	0.261		0.012					[1]
335	Tatun 5	Taiwan	G	93.1	0.509	0.000	0.118	0.000	6.280		0.001					[1]
336	Tatun 3	Taiwan	G	91.6	1.657	0.006	0.668	0.030	6.043		0.003					[1]
337	Tatun 2	Taiwan	G	78.1	2.361	0.001	1.079	0.001	18.483		0.003					[1]
338	Tatun 7	Taiwan	G	86.1	0.927	0.000	1.155	0.175	11.657		0.001					[1]
339	Tatun 1	Taiwan	G	72.0	8.152	0.786	6.410	0.096	12.498		0.069					[1]
340	Beryl Spring	USA	V	95.2	0.313	0.097	0.019	0.111		0.001	0.008	-2.51			12	[21]
341	Sulphur Caldron2	USA	V	99.2	0.168	0.001	0.026	0.113		0.002	0.002	-1.91			15.4	[21]
342	Yellowstone 12	USA	V	97.7	0.262	0.002	0.027	0.195	1.803		0.006					[1]
343	Yellowstone 1	USA	V	98.8	0.197	0.001	0.028	0.142	0.740		0.003					[1]
344	Mud Geyser	USA	V	100.0	0.168	0.002	0.033	0.057		0.002	0.002	-1.96			16.2	[21]
345	Roaring Mountain2	USA	V	96.0	0.444	0.105	0.036	0.184		0.017	0.010	-3.36			2	[21]
346	Yellowstone 3	USA	V	99.0	0.193	0.000	0.037	0.074	0.643		0.003					[1]

ID	SITE	COUNTRY	TYPE	CO_2 %	N_2 %	O_2 %	CH_4 %	H_2 %	H_2S %	He %	Ar %	$\delta^{13}C$ CO_2	$\delta^{13}C$ CH_4	$\delta^{2}H$ CH_4	R/Ra	Ref
347	Mud Geyser	USA	V	99.8	0.200	0.001	0.039	0.066		0.002	0.003	-2.09			16.5	[21]
348	Yellowstone 11	USA	V	98.5	0.213	0.001	0.041	0.079	1.154		0.003					[1]
349	Yellowstone 5	USA	V	96.5	0.535	0.002	0.044	0.148	2.759		0.014					[1]
350	Crater Hills	USA	V	97.5	0.203	0.001	0.051	0.011		0.003	0.004	-2.01			10.7	[21]
351	Yellowstone 6	USA	V	97.4	0.245	0.001	0.056	0.016	2.272		0.005					[1]
352	Guardian	USA	V	90.3	2.068	0.124	0.091	0.265		0.002	0.027	-2.21			8.76	[21]
353	Yellowstone 2	USA	V	96.0	1.633	0.001	0.196	0.545	1.600		0.041					[1]
354	Yellowstone 10	USA	V	96.5	0.450	0.003	0.205	0.703	2.018		0.011					[1]
355	Pocket Basin	USA	V	94.5	8.400	0.880	0.257	0.217		0.004	0.118				2.98	[21]
356	Yellowstone 7	USA	V	77.1	17.601	2.606	0.287	0.011	2.112		0.213					[1]
357	Yellowstone 8	USA	V	95.4	0.332	0.001	0.296	0.151	3.821		0.008					[1]
358	Norris Canyon Rd	USA	V	95.8	0.388	0.001	0.305	0.017		0.005	0.009	-2.05			5.28	[21]
359	Yellowstone 13	USA	V	96.6	0.555	0.001	0.353	0.025	2.399		0.014					[1]
360	Yellowstone 9	USA	V	95.7	1.598	0.008	0.355	0.341	1.989		0.043					[1]
361	Bison Flat	USA	V	96.2	0.381	0.002	0.378	0.163		0.006	0.009	-2.87			4.26	[21]
362	Fountain Paint Pot	USA	V	87.3	2.557	0.039	0.833	0.006		0.006	0.064	-1.68			6.38	[21]
363	Yellowstone 14	USA	V	93.6	3.012	0.005	0.928	0.008	2.360		0.079					[1]
364	Yellowstone 4	USA	V	90.4	0.202	0.005	2.997	1.932	3.334		0.001					[1]
365	Behind Inkpot	USA	V	89.0	0.279	0.008	4.857	2.724		0.002	0.001	-2.65			4.65	[21]

Tab.1: Molecular and isotopic composition of the gas related to volcanoes and hydrothermal geothermal systems. Gas composition is in vol.%. Isotopic data: $\delta^{13}C$: ‰ VPDB; $\delta^{2}H$: ‰ VSMOW; R/Ra© = ($^{3}He/^{4}He$)sample/(3He/4He)atmosphere; Ra= 1.39 x 10-6. Type: V= volcano; G= hydrothermal geothermal system. Empty cells mean "not measured". [1] Tassi et al., 2010; [2] Aguilera et al., 2011; [3] Snyder et al., 2003; [4] Tassi et al., 2005; [5] Welhan & Lupton, 1987; [6] Botz et al., 1996; [7] Fridriksson et al., 2016,; [8] Tassi et al., 2012; [9] Cinti et al., 2017; [10] Cinti et al., 2014; [11] Minissale et al., 1997 (a); [12] Cinti et al., 2011; [13] Minissale et al., 1997; [14] Minissale, 2004; [15] Kiyosu, 1983; [16] Joseph et al., 2011; [17] Goff, Janik, 2002; [18] Giggenbach et al., 1993 (a); [19] Giggenbach et al., 1993 (b); [20] Reyes et al., 1993; [21] Chiodini et al., 2012.

Supplementary References

Aguilera F., Tassi F., Darrah T., Moune S., Vaselli O. (2011) - Geochemical model of a magmatic–hydrothermal system at the Lastarria volcano, northern Chile. Bull Volcanol. 74:119–134 DOI 10.1007/s00445-011-0489-5

Botz R., Stüben D., Winckler G., Bayer R., Schmitt M., Faber E. (1996) - Hydrothermal gases offshore Milos Island, Greece. Chemical Geology 130, 161-173

Chiodini G., Caliro S., Lowenstern J.B., Evans W.C., Bergfeld D., Tassi F., Tedesco D. (2012) - Insights from fumarole gas geochemistry on the origin of hydrothermal fluids on the Yellowstone Plateau. Geochimica et Cosmochimica Acta 89, 265–278, http://dx.doi.org/10.1016/j.gca.2012.04.051

Cinti, D., Procesi, M., Tassi, F., Montegrossi, G., Sciarra, A., Vaselli, O., Quattrocchi, F., 2011. Fluid geochemistry and geothermometry in the western sector of the Sabatini volcanic district and the Tolfa Mountains (Central Italy). Chem. Geol. 284, 160-181.

Cinti, D., Tassi, F., Procesi, M., Bonini, M., Capecchiacci, F., Voltattorni, N., Vaselli, O., Quattrocchi, F., 2014. Fluid geochemistry and geothermometry in the unexploited geothermal field of the Vicano-Cimino Volcanic District (Central Italy). Chem. Geol. 371, 96-114.

Cinti, D.; Tassi, F.; Procesi, M.; Brusca, L.; Cabassi, J.; Capecchiacci, F.; Delgado Huertas, A.; Galli, G.; Grassa, F.; Vaselli, O.; et al. Geochemistry of hydrothermal fluids from the eastern sector of the Sabatini Volcanic District (central Italy). Appl. Geochem., 84, 187–201.

Fridriksson T., Padrón E., Óskarsson F., Pérez N.M. (2016) - Application of diffuse gas flux measurements and soil gas analysis to geothermal exploration and environmental monitoring: Example from the Reykjanes geothermal field, SW Iceland. Renewable Energy 86 (2016) 1295e1307, http://dx.doi.org/10.1016/j.renene.2015.09.034

Giggenbach W.F., Sano Y. And Wakita H. (1993) (a) - Isotopic composition of helium, and CO2 and CH, contents in gases produced along the New Zealand part of a convergent plate boundary. Geochimca et Cosmochimica Acta Vol. 57. pp. 3427-345.

Giggenbach W.F. (1993) (b) - Redox control of gas compositions in Philippine volcanic-hydrothermal systems. Geothermics, Vol. 22, No. 5/6, pp. 575-587.

Goff F., Janik C.J. (2002) - Gas geochemistry of the Valles caldera region, New Mexico and comparisons with gases at Yellowstone, Long Valley and other geothermal systems. Journal of Volcanology and Geothermal Research 116, 299-323.

Joseph E.P., Fournier N., Lindsay J.M., Fischer T.P. (2011) - Gas and water geochemistry of geothermal systems in Dominica, Lesser Antilles island arc. Journal of Volcanology and Geothermal Research 206, 1–14, doi:10.1016/j.jvolgeores.2011.06.007

Kiyosu Y. (1983) - Hydrogen isotopic compositions of hydrogen and methane from some volcanic areas in northeastern Japan. Earth and Planetary Science Letters, 62, 41-52.

Minissale A., Magro G., Vaselli O., Verrucchi C., Perticone I., (1997) (a) - Geochemistry of water and gas discharges from the Mt. Amiata silic complex and surronding areas (Central Italy). Journal of Volcanology and Geothermal Research 79, 223-251.

Minissale A., Evans W.C., Magro G., Vaselli O. (1997) (b) - Multiple source components in gas manifestations from north-central Italy. Chemical Geology 142, 175-192

Minissale A. (2004) - Origin, transport and discharge of CO_2 in central Italy. Earth-Science Reviews 66, 89–141, doi:10.1016/j.earscirev.2003.09.001

Reyes A.G., Giggenbach W.F., Saleras J.R.M., Salonga N.D. and Vergara M.C. (1993) - Petrology and geochemistry of alto peak, a vapor-cored hydrothermal system, Leyte province, Philippines. Geothermics, Vol. 22, 5/6, pp. 479-519.

Snyder G., Poreda R., Fehn U., Hunt A. (2003) - Sources of nitrogen and methane in Central American geothermal settings: Noble gas and 129I evidence for crustal and magmatic volatile components. G3 Vol. 4, 1, 9001, doi:10.1029/2002GC000363

Tassi, F., Martinez, C., Vaselli, O., Capaccioni, B., Viramonte, J. (2005) - Light hydrocarbons as redox and temperature indicators in the geothermal field of El Tatio (northern Chile). Appl. Geochem., 20, 2049–2062.

Tassi F., Montegrossi G., Capechiacci F. and Vaselli O. (2010) - Origin and Distribution of Thiophenes and Furans in Gas Discharges from Active Volcanoes and Geothermal Systems. Int. J. Mol. Sci., 11, 1434-1457; doi:10.3390/ijms11041434

Tassi F., Fiebig J., Vaselli O., Nocentini M. (2012) - Origins of methane discharging from volcanic-hydrothermal, geothermal and cold emissions in Italy. Chemical Geology 310–311 (2012) 36–48. doi:10.1016/j.chemgeo.2012.03.018

Welhan J.A. and Lupton J.E. (1987) - Light Hydrocarbon Gases in Guaymas Basin Hydrothermal Fluids: Thermogenic Versus Abiogenic Origin. The American Association of Petroleum Geologists Bulletin, vol. 71, 2, 215-223.